

## RESEARCH ARTICLE

# Assessing impacts of alternative land use strategies on water partitioning, storage and ages in drought-sensitive lowland catchments using tracer-aided ecohydrological modelling

Shuxin Luo<sup>1,2</sup>  | Doerthe Tetzlaff<sup>1,2,3</sup> | Aaron Smith<sup>2</sup> | Chris Soulsby<sup>3,2</sup> 

<sup>1</sup>Geography Institute, Humboldt University of Berlin, Berlin, Germany

<sup>2</sup>IGB Leibniz-Institute of Freshwater Ecology and Inland Fisheries Berlin, Berlin, Germany

<sup>3</sup>Northern Rivers Institute, School of Geosciences, University of Aberdeen, Aberdeen, UK

## Correspondence

Shuxin Luo, Geography Institute, Humboldt University of Berlin, Berlin, Germany.  
Email: [shuxin.luo@igb-berlin.de](mailto:shuxin.luo@igb-berlin.de)

## Funding information

Einstein Stiftung Berlin, Grant/Award Number: ERU-2020-609; Leverhulme Trust

## Abstract

Continuing negative rainfall anomalies, coupled with climate change projections of increased drought severity and frequency, drive an urgent need to increase resilience and integration in land and water management strategies in many regions of the world. However, complex interactions between land cover change, ecohydrological partitioning and water availability are difficult to quantify, especially at different temporal and spatial scales. In conjunction with local stakeholders, we developed plausible, alternative land use scenarios (including forest diversification and agroforestry schemes) based on the existing four primary land use types (i.e., conifer and broad-leaved forests, arable agriculture, and pasture) in a 66 km<sup>2</sup> drought-sensitive catchment in northern Germany. We used modelling to evaluate spatial and temporal changes in water flux partitioning, storage and ages. The spatially-distributed, tracer-aided ecohydrological model, ECH<sub>2</sub>O-iso, calibrated using hydrometric, ecohydrological and isotopic data at daily time steps from 2007 to 2019 was used in this assessment. The results showed that replacing conifer forests with uneven-aged mixed forests with younger broad-leaved trees had the greatest potential for reducing total evapotranspiration and increasing groundwater recharge. For coniferous forests, a 50% increase in the proportion of broad-leaved trees was projected to result in an 11% increase in groundwater recharge across the catchment. The mixed-forest management alternatives also reduced groundwater turnover times, which would support more rapid recovery of soil moisture and groundwater stores following droughts. This study demonstrates that such an ecohydrological modelling approach has the potential to contribute useful science-based evidence for policy makers allowing quantitative assessment of potential land use effects on water availability and effective communication with stakeholders.

## KEYWORDS

drought, ecohydrological modelling, land use, tracers, water age, water partitioning

## 1 | INTRODUCTION

Over the past decade, dry, warm periods of increased severity and longevity have resulted in water scarcity problems in many parts of the world. In the lowlands of central Europe, for example, the 2018 drought resulted in widespread reductions in crop yields, forest damage, low groundwater levels and cessation of streamflow (Kowalski et al., 2022; Schuldt et al., 2020). Such droughts are expected to occur more frequently as a consequence of climate change (Grillakis, 2019). Ongoing negative rainfall anomalies and climate projections for future warmer, drier conditions have focused policy making towards building resilience in land and water management (e.g., the low water concept in Germany (MLUK-Ministerium für Landwirtschaft, 2021) and drought management plans in Spain (Estrela & Vargas, 2012)). As evapotranspiration is usually the dominant water flux in drought sensitive areas, water partitioning under different land uses becomes a key issue in terms of what land cover will be sustainable and how it will impact other ecosystem services such as groundwater recharge and streamflow generation.

The flat lowlands of the Northern European Plain cover an extensive area where the fertile soils are intensively farmed for arable production, whereas wetter and drier soils support pasture and forests, respectively (Bogucki, 1996; Jones et al., 2012). On the best agricultural land, high value cereal crops such as wheat and maize have been grown. In forests, planting conifers were favoured because of large demands for softwoods and high profitability from their rapid growth and short rotation periods (Johann, 2006). In northern and central Europe this resulted in extensive monocultures of arable crops and fast-growing conifer forests predominantly Scots pine (*Pinus sylvestris*). Such forests were converted from more natural mixed forests, including broadleaves such as oak (*Quercus robur*) and beech (*Fagus sylvatica*) (Felton et al., 2010; Johann, 2006). These monocultures lack biodiversity and can reduce the stability of ecosystems, with less resilience to external disturbances such as drought, wind and fire damage and insect infestation; resulting in potentially reduced yields (de Groot et al., 2021; Wright et al., 2021). Consequently, there is growing interest in replacing monocultures to enhance sustainability and resilience in the face of climate change (Liu et al., 2018).

Recent studies have shown that alternative land uses such as agroforestry and mixed forests are promising land management strategies with many benefits including increased ecosystem biodiversity, and optimizing water use in relation to competing needs (Kuyah et al., 2019; Landgraf et al., 2023; Wright et al., 2021; Wu, Kuang, et al., 2021). Increasing the proportion of broad-leaved trees is an extensively studied strategy for such adaptations (Astrup et al., 2018; Schwaab et al., 2020). In addition to mixed-species planting, uneven-aged alternatives with variable proportions of young and mature trees have also been shown to reduce vulnerability to future risks (Kuuluvainen & Gauthier, 2018; Savilaakso et al., 2021). However, there is a lack of accessible and robust tools to generate advanced spatio-temporal understanding of potential impacts of different land use management alternatives on hydrological fluxes and water balance components. In terms of water cycle variability, this requires

quantitative understanding of how ecohydrological water partitioning changes, as well as how this affects water storage in the subsurface (i.e., soil moisture and groundwater) and the generation of streamflow. This is crucial in complex, heterogeneous catchment landscapes to plan spatial arrangements of sustainable and drought resilient land cover types (Neill et al., 2021).

Ecohydrological models are invaluable for quantifying how different land use and vegetation communities partition rainfall into “green” water fluxes that return moisture to the atmosphere and “blue” water fluxes to groundwater recharge and streamflow generation (Fatichi et al., 2016). Such models play a key role in improving understanding of processes and effects which cannot be easily monitored and thus, provide an evidence base to policy makers (Vose et al., 2011). These models are increasingly sophisticated and can specifically conceptualize the dominant processes determining land cover effects on water partitioning by parameterising key vegetation influences, such as canopy characteristics (e.g., leaf area index, canopy interception capacity, stomatal resistance etc.), rooting properties (e.g., densities, depth distributions etc.) and management effects (Guswa et al., 2020). These land use controls can be conceptualized at multiple scales (plant to large catchment). Spatially distributed models can link variations in soil properties, land use and so forth and water availability in the landscape. Importantly, incorporation of environmental tracers, such as stable water isotopes, into such ecohydrological models is a new development that can help constrain process uncertainty and improve model performance (Kuppel et al., 2018; Smith et al., 2021). This is because: (a) accurate tracking of a conservative tracer through an ecohydrological system and landscape can quantify the water storage that water fluxes mix with more accurately than hydrometrically-based models (Birkel et al., 2011); (b) such tracking can constrain estimates of ages (i.e., the average time elapsed since water entered the system as rainfall) of water fluxes and storages from different landscape compartments (Hrachowitz et al., 2013); and (c) capturing the phase changes of water in isotopic fractionation can help resolve evapotranspiration into its components of canopy interception, soil evaporation and transpiration (Kuppel et al., 2020).

Recent use of such tracer-aided ecohydrological models has provided invaluable insights into how different vegetation and land use affect the interactions between water fluxes, storage and ages across a contrasting range of complex, heterogeneous landscapes (e.g., Douinot et al., 2019; Knighton et al., 2020; Kuppel et al., 2018; Smith et al., 2021; Yang et al., 2021). Such models allow quantitative assessment of the likely effects of land use change on water availability as they are more nuanced than traditional hydrological models in simulating storage changes at multiple spatial and temporal scales (Smith, Tetzlaff, Maneta, & Soulsby, 2022a). For example, effects of different species, management (i.e., age and density of vegetation) and landscape topology can be explored (Neill et al., 2021). Consequently, such models have untapped potential as decision support tools for land and water managers; as well as providing powerful visualizations for communicating the spatio-temporal implications of land use change on water availability to stakeholders in a process-based way (Smith, Tetzlaff, Maneta, & Soulsby, 2022b).

Here, we applied the spatially-distributed, tracer-aided ecohydrological model EcH<sub>2</sub>O-iso to assess the water use and explore the associated impacts of alternative land use changes in the 66 km<sup>2</sup> Demnitzer Millcreek catchment (DMC) in north-east Germany. DMC lies in a mixed land use lowland, drought sensitive landscape that was severely impacted by the 2018 European drought. Subsequent ongoing drought has resulted in urgent consideration of potential land use changes designed to better balance crop and timber production with reduced green water fluxes, increased water retention in the landscape and maintenance of blue water fluxes to groundwater recharge and streamflow generation. Our overarching goal therefore was to assess the ecohydrological implications for such land use changes (with focus on a move from traditional arable farming and conifer forests to increased agroforestry and mixed forest) in terms of spatio-temporal differences in water flux partitioning, storage dynamics and ages. We used multi-criteria model calibration to specifically address the following three research questions.

- How do land use changes affect green and blue water flux partitioning across a complex landscape?
- What are the implications for water storage and age dynamics under different plausible agroforestry and mixed-forest land use scenarios?
- Which land management options are most drought-resilient in terms of enhancing water storage and reducing water loss from evapotranspiration, especially in the context of successive years of drought?

In addressing these questions and applying EcH<sub>2</sub>O-iso to drought-related land use changes as a “proof of concept”, we also sought to highlight uncertainties with the modelling, as well as assessing current limitations with such an approach and future research needs to further improve ecohydrological modelling approaches.

## 2 | STUDY SITE

The land use change assessment was undertaken for a landscape typical of the North European Plain (NEP) in northern Germany. The study site DMC is approximately 50 km SE of Berlin (Figure 1a). Established over 30 years ago, DMC is an environmental observatory with data on hydroclimate, hydrodynamics and water quality. Its characteristics have been extensively described elsewhere, so only a concise summary follows (for details see Gelbrecht et al., 1998, 2005; Kleine et al., 2021; Smith et al., 2021). DMC (66 km<sup>2</sup>) has a complex land use pattern that is representative of the NEP, dominated by monocultures of agricultural crops (e.g., maize, wheat etc.) mainly in the North and coniferous forest (mainly Scots pine) dominating the south (Figure 1a); though small areas of broadleaved forests (mainly oak and beech) and pastures (for sheep and cattle grazing) are also present. The topography is representative of the NEP (Böse & Brande, 2010) with gentle slopes (steepest in the headwaters) and limited relief variation (30–90 m.a.s.l) (Figure 1b). Silty brown earth and sandy podzols are the

dominant soil types, supporting arable crops and forests, respectively (Figure 1c). Substantial areas of poorly drained peat and gley soils fringe the river network and support pasture. The soils are predominantly underlain by glacial tills and the water table is typically 1–3 m below the surface (Ying et al., 2024).

The climate is humid continental. Average annual precipitation is ~580 mm, which has declined by ~20 mm per year over the last decade (Smith, Tetzlaff, Maneta, & Soulsby, 2022a). Moreover, in recent years, negative precipitation anomalies have become more frequent, and annual precipitation in dry years can be about half of that in wet years (German Meteorological Service, 2020). Mean annual temperature is ~9.8°C with a slightly increasing trend over the past three decades (Wu, Tetzlaff, et al., 2021). DMC also experiences high potential evapotranspiration (PET) (~600 mm Pa). The combined effects of low rainfall and high PET result in a climate-sensitive hydrological regime with runoff coefficients <10%. Streamflow is groundwater-dominated and shows distinct seasonality with flows increasing in winter as groundwater recharge raises the water table (typically by ~1 m) and declining in spring and summer as ET increases and recharge declines (Ying et al., 2023). Storm runoff is superimposed on this seasonality, especially in heavier winter rainfall, by the activation of artificial drains in more poorly drained soils and overland flow from wet riparian soils (Wu et al., 2022).

Since the 1990s, catchment management interventions have sought to reverse historic drainage schemes and retain water in the landscape longer. These include re-naturalization of some sections of river channels and restoration of wetlands; though after 2006, recolonization by beavers (*Castor fibre*) accelerated natural re-wilding (Smith et al., 2020). In recent years, patches of alternative land uses such as agroforestry and use of syntropic agriculture have been established on an experimental basis (Figure 1a) (Landgraf et al., 2023).

## 3 | METHODS

### 3.1 | Mechanics of the EcH<sub>2</sub>O-iso model in ecohydrological analysis

EcH<sub>2</sub>O-iso is an extension of the ecohydrological model EcH<sub>2</sub>O, which adds a tracer module that tracks stable water isotopes ( $\delta^2\text{H}$  and  $\delta^{18}\text{O}$ ) and their transport and phase-change fractionation in water fluxes (Kuppel et al., 2018). Concurrent time stamping of precipitation inputs allows estimations of water ages in each model storage and flux (Figure 2). The EcH<sub>2</sub>O-iso model has been successfully applied to catchments with contrasting geographical and ecohydrological characteristics in Germany (Douinot et al., 2019; Yang et al., 2021), the UK (Neill et al., 2021), Sweden (Smith et al., 2019) and the US (Knighton et al., 2020); applications also include a wide range of temporal scales (e.g., Smith, Tetzlaff, Landgraf, et al., 2022).

Briefly, the governing equations are solved for each vegetation type at each time step and each model grid for the four major components (i.e., energy, water, biomass and tracer). The integrated energy-water-vegetation-tracer model provides a mechanistic insight into

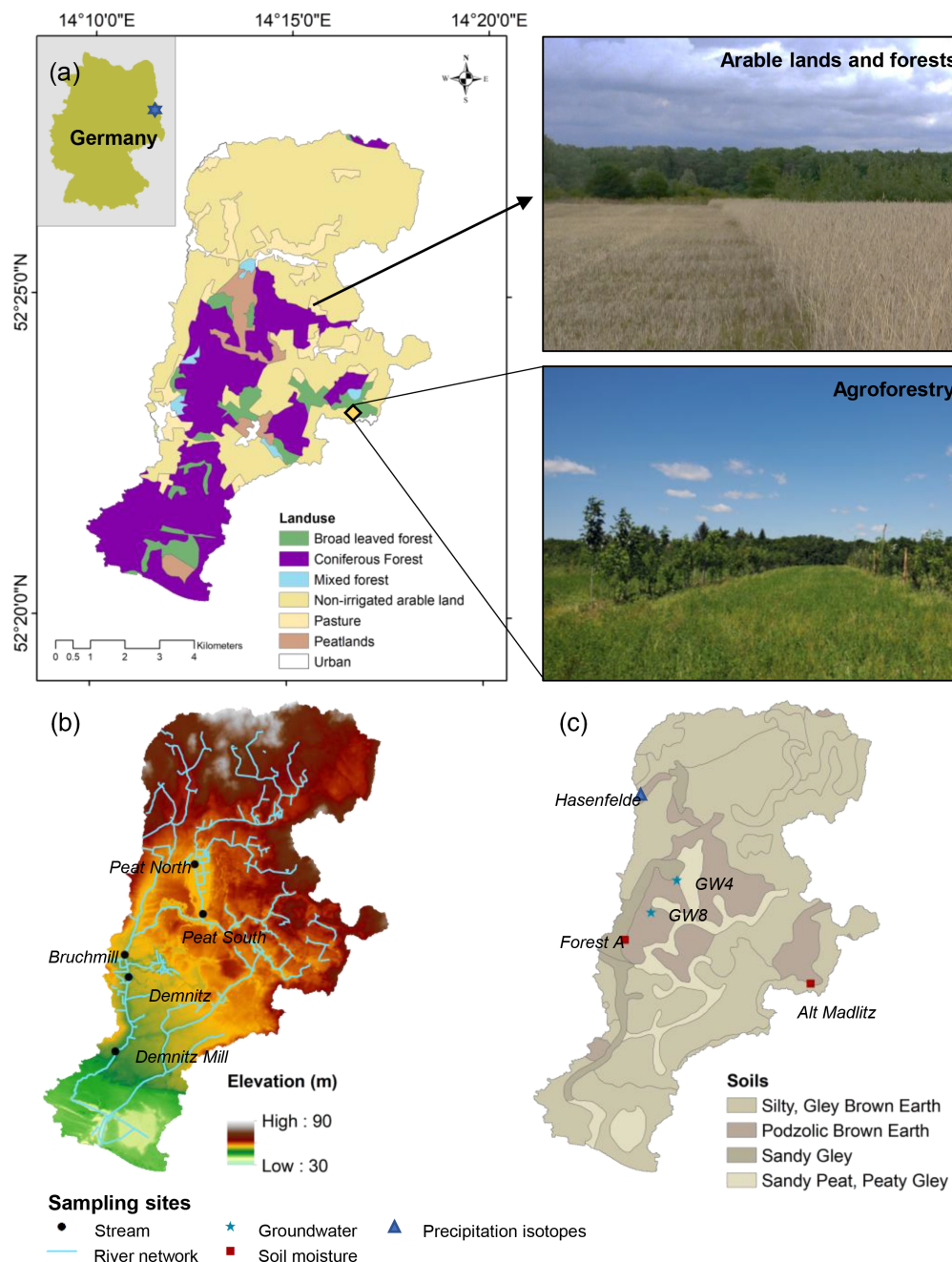


**FIGURE 1** The location of the Demnitzer Millcreek catchment and: (a) land use (b) elevation with discharge and stream sampling sites for stream isotopes (c) soils with groundwater and soil sampling sites.

how land cover impacts ecohydrological partitioning in response to external climatic and hydrological drivers. The model is solved using a vertical scheme with multiple layers from the canopy to soil surface to three subsurface layers. The canopy processes are driven by precipitation, incoming radiation, air temperature, relative humidity and wind-speed, and impact the energy exchanges between canopy and land surface, evapotranspiration, soil water availability and soil water potential energy. The canopy-level processes can be characterized by three key equations in terms of canopy energy balance (Equation 1), root zone water balance (transpiration, Equation 2) and soil matric potential (Equation 3).

The energy balance equation assumes that vegetation has negligible heat capacity and allocates the available energy (net radiation,  $R_{nc}$ )

to conductive sensible heat flux ( $H$ ) and latent heat flux between canopy and atmosphere. Latent heat fluxes are associated with evaporation of canopy intercepted water (LE) and vegetation transpiration (LET). All the terms in Equation (1) are nonlinearly related to canopy temperature ( $T_c$ ), which is determined by using Newton-Raphson method to find the root of Equation (1).

$$R_{nc}(T_c) + LE(T_c) + LET(T_c, \Psi_s) + H(T_c) = 0. \quad (1)$$

Net radiation absorbed by each vegetation type in the grid cell is derived from the sum of incoming shortwave radiation ( $R_s$ ) and long-wave radiation ( $R_l$ ) and deduction due to canopy emission of longwave radiation:



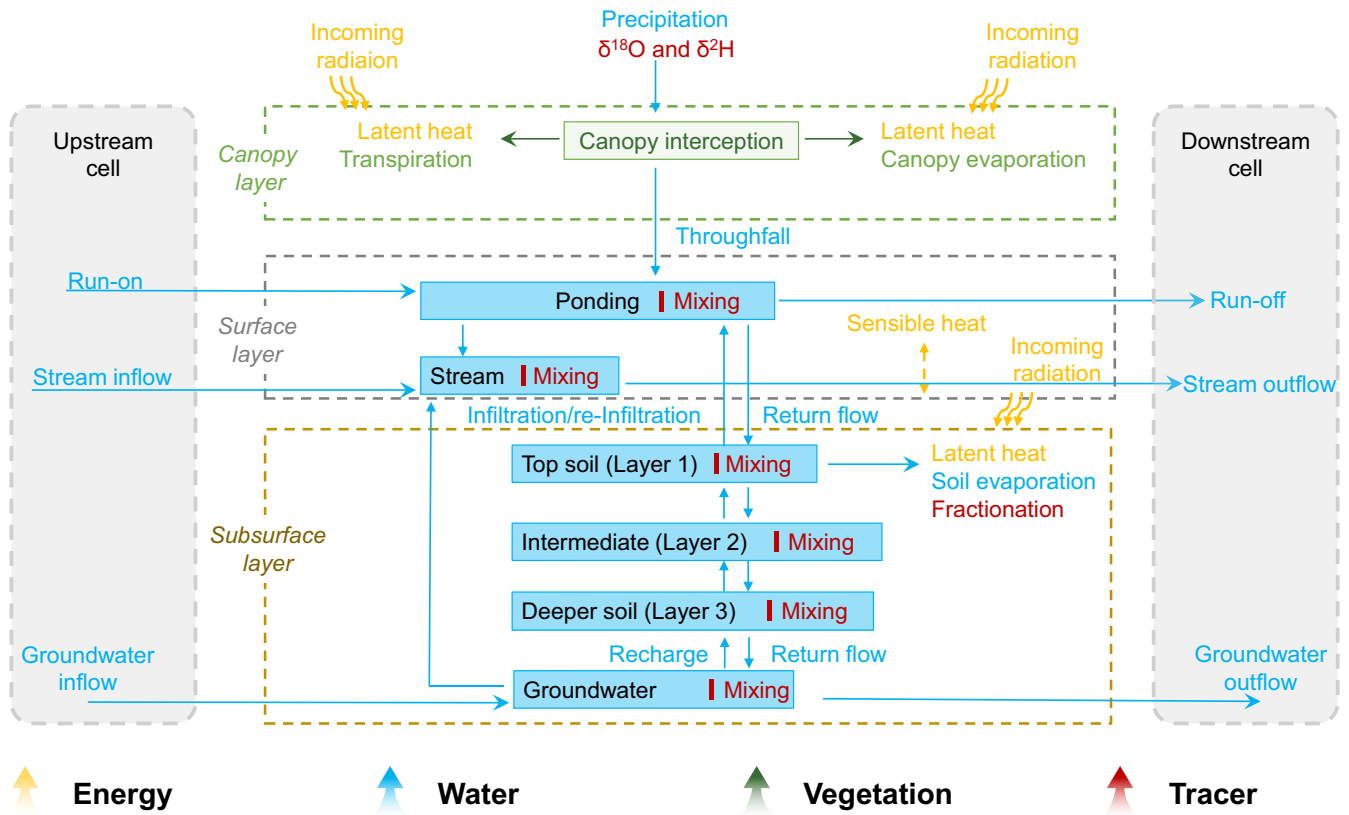


FIGURE 2 Schematic diagram of EcH<sub>2</sub>O-iso.

$$R_{nc}(T_c) = R_s(1 - \alpha_{soil})(1 - e^{-K_{Beers} \cdot LAI}) + \epsilon_c R_l - (\epsilon_c \sigma T_c^4), \quad (1.1)$$

where  $\alpha_{soil}$  denotes soil albedo;  $K_{Beers}$  denotes the light extinction coefficient (Beer's law); LAI denotes the leaf area index of the vegetation;  $\epsilon_c$  denotes the emissivity and absorptivity of the vegetation and  $\sigma$  denotes the Stefan-Boltzmann constant. The parameters in bold are those highlighted by Morris sensitivity analysis and calibrated in this study as described in Section 3.2 and Table S1.

Latent heat flux consumed for evaporation of canopy-intercepted water is controlled by maximum intercepted water ( $CWS_{max}$ ):

$$LE(T_c) = \frac{\rho_a c_a (e_a - e_c^*(T_c) (rH + \frac{1-rH}{CWS_{max}} \cdot CWS))}{\gamma \times r_a(W)}, \quad (1.2)$$

where  $\rho_a$  denotes density of air;  $c_a$  denotes the specific heat capacity of air;  $e_a$  denotes air vapour pressure at air temperature ( $T_a$ );  $e_c^*$  denotes the saturation vapour pressure of leaf surface at  $T_c$ ;  $rH$  denotes the relative humidity;  $CWS$  and  $CWS_{max}$  denote the current canopy water storage and its maximum, respectively;  $\gamma$  denotes psychrometric constant;  $r_a$  denotes aerodynamic resistance between the leaf surface and atmosphere and is a function of wind speed ( $W$ ).

Latent heat flux used by vegetation transpiration is calculated from the difference between vapour pressure at atmosphere and leaf surface. LET is constrained by aerodynamic and leaf stomatal resistance. Stomatal conductance controlling transpiration is estimated

using a Jarvis-type multiplicative model (Jarvis, 1976), incorporating factors such as shortwave radiation ( $f(R_s)$ ), air temperature ( $f(T_a)$ ), vapour pressure deficit ( $f(vpd)$ ,  $gs_{vpd}$ ) and soil water potential ( $f(\Psi_s)$ ).

$$LET(T_c, \Psi_s) = \frac{\rho_a c_a (e_a - e_c^*(T_c) \cdot rH)}{\gamma(r_a(W) + r_c(\Psi_s))}. \quad (1.3)$$

$$r_c(\Psi_s) = [gs_{max} \cdot LAI \cdot f(R_s) \cdot f(T_a) \cdot f(vpd) \cdot f(\Psi_s)]^{-1}, \quad (1.4)$$

where  $r_c$  denotes the canopy resistance (reverse of canopy conductance);  $gs_{max}$  denotes maximum stomatal conductance;  $gs_{vpd}$  denotes the vapour pressure deficit sensitivity for conductivity; LAI is used to scale stomatal conductance to canopy conductance.

Sensible heat flux between different canopy is calculated as:

$$H(T_c) = \frac{\rho_a c_a (T_a - T_c)}{r_a}. \quad (1.5)$$

The water balance follows the energy balance structure and is multilayered with a vegetation canopy, soil surface and three subsurface layers (Figure S1). Throughfall occurs when precipitation exceeds maximum canopy storage ( $CWS_{max}$ ), which is limited by LAI. The infiltration rate is estimated using the Green-Ampt approximation of the Richards equation. The root zone water balance is calculate considering the infiltration contribution to soil moisture (Equation 2). The left term is the transpiration flux derived from latent heat flux, whereas

the right term represents changes in soil water flux in the root zone over one time step.

$$\frac{\text{LET}(T_c, \psi_s)}{\rho_w \lambda_v} = \frac{S_{t+1} - S_t}{\Delta t} (\eta - \theta_r) \cdot d_{95}, \quad (2)$$

where  $\rho_w$  denotes density of water;  $\lambda_v$  denotes the latent heat of vaporization;  $S_t$  and  $S_{t+1}$  respectively denote the degree of saturation at the beginning and end of a time step ( $\Delta t$ );  $\eta$  denotes the soil porosity;  $\theta_r$  denotes the residual soil water content;  $d_{95}$  denotes the soil depth with 95% root distribution.

The transpiration fraction of water taken up from each soil layer (three soil layers in EcH<sub>2</sub>O-iso) is not only determined by the proportion of the water content of each soil layer but the  $K_{\text{root}}$  parameter which allocates according to the respective fraction of roots that is assumed to vary exponentially with soil depth (Equation 2.1).  $d_{95}$  is chosen from the smaller between the total soil depth and 95% distribution depth to ensure that the calculated 95% depth does not exceed the total soil depth.

$$\begin{cases} f_{L1} = \frac{1 - e^{-K_{\text{root}} \cdot d_{L1}}}{1 - e^{-K_{\text{root}} \cdot d}} \\ f_{L2} = \frac{e^{-K_{\text{root}} \cdot d_{L1}} - e^{-K_{\text{root}} \cdot (d_{L1} + d_{L2})}}{1 - e^{-K_{\text{root}} \cdot d}} \\ f_{L3} = 1 - f_{L1} - f_{L2} \\ d_{95} = \min \left( d, \frac{\log_2(0.05 + 0.95e^{-K_{\text{root}} \cdot d})}{-K_{\text{root}}} \right) \end{cases}, \quad (2.1)$$

where  $f_{L1}$ ,  $f_{L2}$ ,  $f_{L3}$  denote the root fraction in three distinct soil layers, namely L1, L2, and L3;  $d_{L1}$  and  $d_{L2}$  denote the respective soil depths of L1 and L2;  $d$  denotes the total soil depth;  $K_{\text{root}}$  denotes the exponential parameter that controls the root distribution of each vegetation type in the grid cell.

Soil water potential related to the canopy energy balance and root zone water balance is calculated by using the Brooks-Corey parameter and air entry pressure ( $\lambda_{\text{BC}}$  and  $\psi_{\text{ae}}$ ).

$$\psi_s = \frac{\psi_{\text{ae}}}{S_{t+1}^{\lambda_{\text{BC}}}}. \quad (3)$$

Subsurface water can move vertically between the three layers and laterally to the next downslope cell when field capacity is exceeded. The latter is conceptualized by a 1D kinematic wave approximation where groundwater flux is proportional to the cell slope and effective hydraulic conductivity ( $K_h$  and  $K_v K_h$ , Equation 4). When groundwater depth exceeds soil storage capacity, upward return flow occurs. Any ponded water on the soil surface (either from infiltration-excess or return flow) is routed laterally to the adjacent downslope cell as overland flow or directly to the channel. Channel routing is estimated using a 1D kinematic wave approach associated with hydraulic parameters ( $M_n$ , Table S1), and re-infiltration is possible.

$$\frac{\partial h_g}{\partial t} + K_h \sin \alpha_x \frac{\partial h_g}{\partial x} + q_{\text{rch}} - q_{\text{rtn}} - q_{\text{cap}} - q_{\text{chan}} = 0, \quad (4)$$

where  $h_g$  denotes the water depth exceeding field capacity;  $t$  denotes time;  $K_h$  denotes effective hydraulic conductivity;  $S_x$  denotes the cell slope;  $x$  denotes distance;  $q_{\text{rch}}$  denotes the recharge flow rate to the saturated layer;  $q_{\text{rtn}}$  denotes the upward return flow rate;  $q_{\text{cap}}$  denotes the rate of water from free gravitational pool to the capillary water pool when soil moisture is below field capacity;  $q_{\text{chan}}$  denotes the rate of water from subsurface to channel.

The tracer module of EcH<sub>2</sub>O-iso, assisting in constraining the uncertainties, applies the assumption of full mixing for all implemented tracked quantities (i.e., isotopes and water age) in each storage compartment. The precipitation age is fixed at zero, whereas the age of each storage compartment (e.g., L1, L2 and L3- representing groundwater) increases at the end of each time step. The concentration of the tracers in the outflow are equal to those of the relevant storage. Isotopic fractionation only occurs during soil evaporation, as canopy evaporation does not interact with the surface and subsurface and throughfall is assumed to have the same isotopic composition of precipitation for the same time step and a water age of zero. The Craig-Gordon model (Craig & Gordon, 1965; Gat, 1995) is used to simulate the isotopic composition changes in the top soil layer during soil evaporation processes.

### 3.2 | Model setup, parametrization and calibration

The hydroclimatic and isotopic data used in modelling are presented in the supporting information (Text S1). The modelling workflow is shown in Figure 2. The model was set up to run at daily time steps for a simulation period of 13 years (Jan 2007–Dec 2019). Grid cells were evenly distributed with a square grid (250 m). Based on existing land use (Figure 1a), four primary types were categorized: conifer forests, broadleaved forests, arable agricultural lands and pasture, with proportions of 29%, 6%, 52% and 13%, respectively (Figure 4a–d). The domain was divided using Thiessen polygons into five climate areas for the inputs using forcing data from five weather stations within 10 km of the catchment. Because of limited spatial variation observed, precipitation isotopes were applied uniformly across the catchment. Leakage to deeper groundwater was allowed at the bottom of the model domain. The first 2 years of simulation were used as a warm-up period to initialize soil moisture, groundwater storage and discharge, in terms of volumes isotopic composition and so forth.

The tracer-aided calibration and validation of EcH<sub>2</sub>O-iso in DMC that has been reported in previous work (see Smith et al. (2021) for details) was used as the basis here. Prior to calibration, a Morris sensitivity analysis was carried out to assess the impact of individual model parameters (Morris, 1991; Sohler et al., 2014), which were specified for each vegetation and soil type. The most sensitive was combined and a total of 100 000 parameter sets sampled using Latin hypercube sampling for Monte Carlo simulations. Multi-criteria calibration of the

sensitive parameters (against soil moisture under four land uses, stream discharge and distributed soilwater, groundwater and streamwater isotopes, evapotranspiration derived from remote-sensing data, transpiration derived from sapflux) across different model compartments was conducted for two simulation periods (2009–2014; 2018–2019) to cover both wet and dry conditions. Model validation was carried out for 2015–2017 at the same sites as calibration (Figure S2 and S3). In Smith et al. (2021), 100 parameter sets with best performance in simulating fluxes, discharge and isotopes were selected by ranking the best overall efficiency using empirical cumulative distribution functions.

As a further constraint on models to be used in land use change scenarios, we used the Tr/ET ratio to reject models where the Tr/ET ratio in the southern forests was markedly lower than in croplands. This is because such models would be inconsistent with a global assessment of Tr/ET ratio from FLUXNET datasets (<https://fluxnet.fluxdata.org>), as reported by Gu et al. (2018), where Tr/ET values for conifer forests (0.3–0.79) and deciduous broad-leaved forests (0.49–0.68) should be similar or higher to those for croplands (0.18–0.48). Consequently, from the initial 100 parameter sets, we refined our selection to 10 sets characterized by higher  $g_{s_{max}}$ , lower  $g_{s_{vpd}}$  and lower  $CWS_{max}$  for conifer and broad-leaved forests (Figure S1a). In addition, we compared our evapotranspiration rates with two FLUXNET stations near Dresden, Germany-situated ~150 km from Berlin and with similar climate and land uses (Figure S1b). The comparison showed a similar ranges and differences to our simulations in conifer forests and croplands. To further test the model, we extended the validation using observed hydrometric and isotopic data spanning 2020–2022. Table S1 shows the most sensitive parameters with their initial ranges used in the calibration process and the final calibrated ranges for the selected 10 parameter sets. Two efficiency criteria were used: Nash–Sutcliffe efficiency (NSE) (Nash & Sutcliffe, 1970) and root mean square error (rMSE). The calibration and validation details are presented in Figure S2 and S3, all exhibiting good agreement with the observations, though increases in soil moisture following the driest summer and autumn in the time series (2022) were overpredicted.

As elaborated in Section 3.1, root distribution is an important indicator that influence the transpiration of different vegetation types and the water balance in the subsurface root zone. The calibrated roots of crops and pastures are mainly distributed in the first layer, whereas the roots of conifers and broadleaved trees are more uniformly distributed in layer 1 and 2 (Figure S4).

### 3.3 | Scenarios and data post-processing

The multi-criteria calibrated and validated model was used as the baseline scenario for the comparison with potential land use change simulated for the same time period. We established “extreme” scenarios that would result from catchment-wide conversion to a single land use (represented by the specific vegetation parameters for each land use) covering the entire catchment (i.e., conifer forests, broad-leaved forests, arable agriculture and pasture) to quantify the resulting changes in water partitioning and ages as a benchmark of maximum impact, which allows us to better interpret the results of more

realistic, intermediate scenarios. Then, in conjunction with local stakeholders (the main land owners of the catchment), we devised alternative water-sensitive land use scenarios. Six plausible, alternative scenarios were explored that would partially replace arable agricultural lands and conifer forests with broad-leaved trees of different ages to assess the impact of these management strategies on water cycle variability at the local and catchment scale (Table 1). To capture the temporal dimension of impacts resulting from land use change and subsequent vegetation growth, two stages (S1 and S2) after conversion were set as snap-shots, featuring young and mature broad-leaved trees, respectively. Changes in forest structure (i.e., proportional vegetation cover, vegetation heights and LAI of broad-leaved trees) were simulated for each stage. For S1, young broad-leaved trees were designated as 8 years old based on the empirical knowledge of the agroforestry experiment site, and the vegetation height was determined by a linear relationship with age. Locally measured LAI of young broad-leaved trees was divided by the LAI of mature broadleaves to obtain a scale factor for LAI. Then, the LAI of young broad-leaved trees was determined by scaling the LAI time series of mature broad-leaved trees using the scale factor (see also Neill et al., 2021). For S2, only vegetation cover was changed. For each stage, we designed three scenarios. For scenario A, 10% of arable agricultural land in each grid cell were replaced with young or mature broad-leaved trees. For scenario B, 50% of conifer forests in each grid cell were replaced with young or mature broad-leaved trees. Scenario C is a combination of scenarios A and B. The work flow chart of the model also summarizes the land use scenario experiments (Figure 3).

Spatial maps of daily outputs of modelled catchment states using the 2009–2019 climate data were analysed for different water fluxes, storage volumes and ages under the land use change scenarios. Green water fluxes include the components of total evapotranspiration (ET), which are transpiration (Tr), soil evaporation (Es) and evaporation of intercepted water (Ei). Blue water fluxes include overland flow (Ov), groundwater recharge (GWr) and lateral groundwater flow (GWf). Although infiltration (Infil) is not strictly a blue water flux, it serves as a crucial source for both green and blue water and is therefore discussed along with blue water fluxes due to our interest on increasing water storage. Ages of streamwater, transpiration and soil evaporation were also quantified. Given the older groundwater ages, groundwater mean residence time ( $MRT = GW \text{ volume} / GW \text{ flux}$ ) was calculated to show the influence of flux changes on storage and local groundwater age (Massmann et al., 2009). Long-term averages were computed for all the scenarios for the simulation period and all the 10 parameter sets at the catchment scale. Time series plots were also generated at the featured sampling sites.

## 4 | RESULTS

### 4.1 | Baseline water flux partitioning and water age

The ECH<sub>2</sub>O-iso model effectively managed uncertainties across various datasets under different land uses. It successfully captured

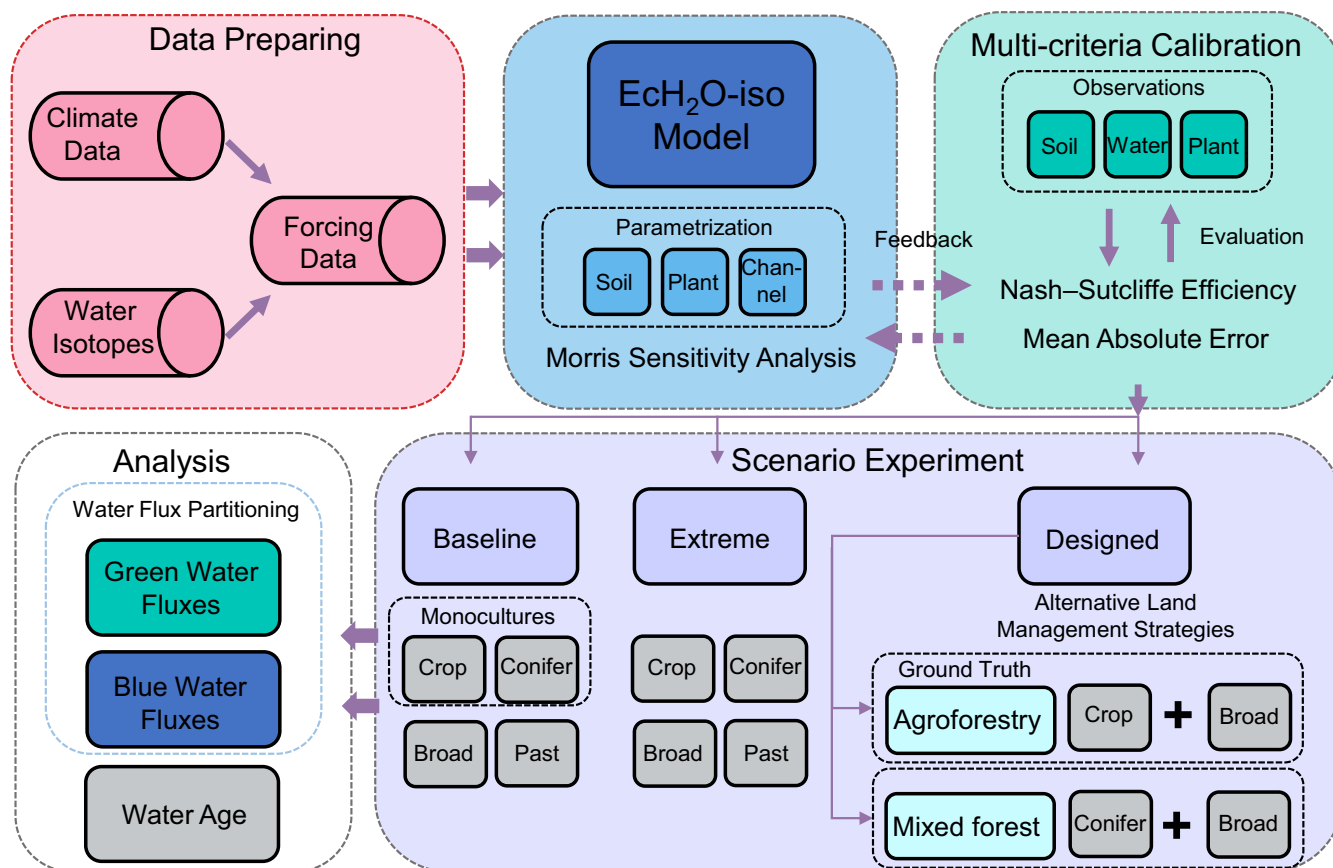


**FIGURE 3** Flow chart of model setup, parameterization, calibration and scenario experiments.

diverse ecohydrological flows (with discharge NSE  $\sim 0.7$  and rMSE  $\sim 0.1 \text{ m}^3 \text{ s}^{-1}$ ; evapotranspiration rMSE  $\sim 1 \text{ mm d}^{-1}$ ) and showed satisfactory performance in simulating soil moisture with rMSE  $\leq 0.05 \text{ m}^3 \text{ m}^{-3}$  for both forest and cropland sites. Isotopic calibrations also showed low uncertainties with rMSE not exceeding 3.6% (Table 2). Figure 4 shows the average catchment-wide distribution of modelled water fluxes and ages under the baseline of current land use. Green water fluxes were highest in the South, where conifer forests predominate (Figure 4e–h). Mean daily ET was high compared with precipitation, especially under forests, reaching  $\sim 2 \text{ mm d}^{-1}$ . Tr averaged  $0.47 \text{ mm d}^{-1}$  across the catchment and was also highest from conifer forests, whereas it was lower in pastures and broad-leaved forests. Because of the lower canopy shading and wetter soils, pastures exhibited higher  $E_s$ . Conversely,  $E_i$  was highest under conifer forests due to the tree canopy.

Blue water fluxes also exhibited high spatial variability. Ov was largely restricted to riparian areas of the headwater tributaries in the NE contributing to the stream channel network. Infil was more uniform, though with a slight decrease under forests in the South due to higher interception losses, with GWr showing a similar pattern. However, high ET limited GWr throughout the catchment, particularly under conifer forests, resulting in significantly lower recharge than Infil. GWf also showed a dependence on land use, with higher values under agriculture in the North.

Groundwater is the largest modelled water storage in DMC and the groundwater MRT was much shorter under arable land in the North ( $\sim 10$  years) and much longer under forests in the South ( $\sim 100$  years), indicating the highest turnover of groundwater under agriculture and lower turnover under conifer forests. Consequently, mean streamwater age was relatively old in the northern headwaters (5–10 years) but then decreased through wetland areas with pasture and peat soils in the central catchment ( $\sim 5$  years), with limited inputs from forested areas. Transpiration water age reflected that of soil-water and was also younger from agriculture ( $< 1$  year) and older from conifer forest ( $\sim 2$  years), indicating deeper, older water was utilized by deeper rooting forests with lower net rainfall. Soil evaporation age was the oldest in the peats and gley soils reflecting pasture distribution.

Figure 5 presents a breakdown of various accumulated modelled green water fluxes across sites, under different land uses with the accumulated precipitation and daily temperature, whereas Table S2 summarizes the average ecohydrological partitioning. The overarching trends observed in these accumulated green fluxes appear to be consistent with the annual precipitation; decreasing with reduced precipitation patterns. During the summer, as energy inputs rise, both accumulated ET and Tr exhibit a more rapid increase. Accumulated ET fluxes of conifer forests are the highest among the four primary land uses, followed by broad-leaved forests, croplands and pastures.



**TABLE 1** Scenarios.

Scenarios	Vegetation type				
	Broad-leaved forest	Conifer forest	Arable agricultural land	Pasture	Young broad-leaved forest
	Proportional aerial coverage				
Baseline	6%	29%	52%	13%	0
S1A	–	–	–10%	–	10% of arable agricultural lands replaced with young broad-leaved trees
S1B	–	–50%	–	–	50% of conifer forests replaced with young broadleaf trees
S1C	–	–50%	–10%	–	10% of arable agricultural lands and 50% of conifer forests replaced with young broad-leaved trees
S2A	10% of arable agricultural lands replaced with mature broad-leaved trees	–	–10%	–	–
S2B	50% of conifer forests replaced with mature broad-leaved trees	–50%	–	–	–
S2C	10% of arable agricultural lands and 50% of conifer forests replaced with mature broad-leaved trees	–50%	–10%	–	–

Note: The—symbols represent proportion changes from existing vegetation type. “Extreme” scenarios are for single vegetation types. S1 is for uneven-aged scenarios, and S2 is for even-aged scenarios.

Specifically, the accumulated Tr fluxes generally mirrored the overall trends of ET across different land uses, except that croplands higher than broad-leaved forests. However, the sequence for accumulated Es fluxes is inverted, with deciduous broad-leaved forests highest particularly in spring prior to leaf out. As for Ei, although the median of conifer forests is lower than that of broad-leaved forests, its upper bound is notably higher (Table S2). Notably, these fluxes exhibit distinct patterns when comparing different land uses, demonstrating the model's skill, and associated uncertainty, in capturing the responses of various land uses to climatic and hydrological changes. Such differences support the integrated effects of the parameterisation described in Section 3.1.

## 4.2 | Temporal changes in discharge and soil moisture

Figure 6 shows the simulated time series of outlet discharge and soil moisture under baseline conditions and for extreme land use changes. Modelling the catchment with only conifer forest land cover resulted in the largest reduction in streamflow over the entire simulation period, with a decline of  $\sim 72 \pm 17\%$  compared with the baseline (Figure 6a). For the extreme scenario of conversion to arable, flows increased by  $\sim 11\%$  compared with baseline (Figure 6b). In both cases, impacts were greatest for low and average flows. Meanwhile, conversions to broad-leaved forests and pastures increased flows by  $39 \pm 72\%$  and  $139 \pm 44\%$  from baseline, respectively. The uncertainties of simulated streamflows generally decreased with decreasing flows, with the lowest uncertainty for the extreme conifer forests scenario.

Unlike the extreme land use changes, the stakeholder-designed land use scenarios showed limited differences in streamflow generation compared to the baseline, especially for scenario A when only 10% of agricultural lands were replaced with broad-leaved forests. For scenarios B and C, modelled discharge slightly increased but in general the differences were subtle (Figure 6c,d). Table S3 summarizes the flow duration curve statistics for baseline and designed scenarios (Figure S5 shows the curves). The differences between the stakeholder-designed and baseline scenarios were greater during low flows that equal to or exceed this discharge 95% of the time, especially for S1 scenarios under the implementation of uneven-aged management. Meanwhile, scenarios B and C also exhibited higher values, indicating an increase in low discharges under the mixed-forest scenarios. Overall, uneven-aged mixed forest of conifer and young broad-leaved trees resulted in most marked changes. The high flows for S1B and S1C increased by  $\sim 12\%$ . The low flows for S1B and S1C increased by 35% and 52%, respectively. The high flows for S2B and S2C increased by 5% and 6%, respectively, and their exceedence curves exhibited similar patterns from high flow to mid-flow. However, the increase in low flows for S2C (13%) was lower than that for S2B (35%). Compared to the baseline scenario, both the high and low flows for scenarios A either remained unchanged or slightly decreased.

The temporal dynamics of discharge responses are strongly linked to land use impacts on catchment storage, which can be indexed by the simulated soil moisture changes in L1 (top 15 cm). Soil moisture in the extreme conifer scenario was lowest and generally lower than the baseline, especially during the growing season (May–September) (Figure 6e). Soil moisture for the extreme arable crop scenario showed similar patterns, and the uncertainties of both conifer and crop were

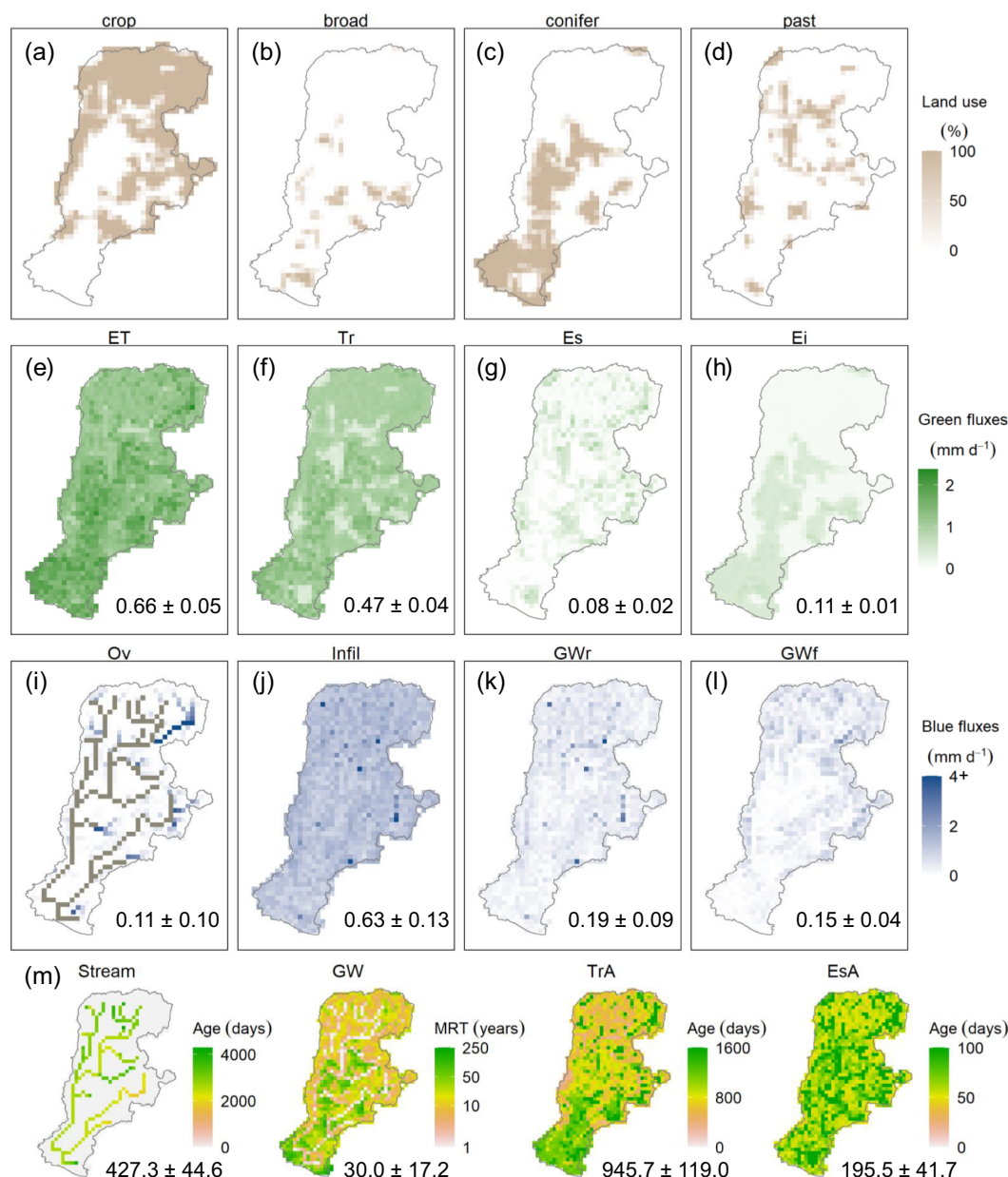


**FIGURE 4** (a–d) Existing land use in the model categorized as four main generic types; arable agriculture (crop), broad-leaved forests (broad), conifer forests (conifer) and pastures (past). Distribution of annual average of modelled (e–h) daily green fluxes, (i–l) daily blue fluxes and (m) water ages of the baseline scenario. The colour bar of blue flux is truncated to emphasize spatial patterns (largest blue flux reached 11.5 mm d<sup>-1</sup> for overland flow). Grey cells on the overland flow sub-figure indicate stream paths without simulated overland flow. Note that groundwater MRT is in years (log scale). The values shown on the subplots are catchment-wide, long-term (2009–2019) average and standard deviations. Ei, evaporation from intercepted water; Es, soil evaporation; EsA, soil evaporation water age; ET, total evapotranspiration; GW, groundwater mean residence time (MRT); GWf, cell-to-cell lateral groundwater flow; GWr, groundwater recharge; Infil, infiltration into the first soil layer (L1, top 15 cm); Ov, cell-to-cell overland flow; Stream, streamwater age; Tr, transpiration; TrA, transpiration water age.

lower than the baseline. An increase in soil moisture in the extreme scenarios only occurred in the pasture scenario, which increased by  $13 \pm 8\%$  on average over the baseline (Figure 6f). The extreme broad-leaved scenario showed no overall difference to the baseline. The simulated soil moisture dynamics for design scenarios were not substantially different to the baseline, though soil moisture slightly increased for scenarios C (Figure 6g,h).

### 4.3 | Catchment-scale spatial patterns in water flux partitioning changes

The temporal changes in streamflow and soil moisture simulation reflect the effects of more complex spatial patterns of modelled changes in green water fluxes under contrasting land use as shown in Figure 5 and Table S2. Compared to the baseline, ET and Tr generally

**TABLE 2** Median calibration efficiency for hydrometric and isotopic data from multicriteria calibration.

	Location	NSE	rMSE
Discharge ( $\text{m}^3 \text{s}^{-1}$ )	Demnitz Mill	0.82	0.07
	Demnitz	0.66	0.11
Evapotranspiration ( $\text{mm d}^{-1}$ )	Forest	-	0.94
	Cropland	-	1.11
Soil moisture ( $\text{m}^3 \text{m}^{-3}$ )	Forest	-	0.05
	Cropland	-	0.06
Stream isotopes (‰)	Demnitz Mill	-	2.98
	Bruch Mill	-	3.6
	Peat North	-	1.88
Soil isotopes (‰)	Forest layer 1	0.65	-
	Forest layer 2	0.11	-
Groundwater isotopes (‰)	GW4	-	2.28

Abbreviations: NSE, Nash–Sutcliffe efficiency; rMSE, root mean square error.

decreased under the stakeholder-driven scenarios, whereas Es and Ei generally increased (Figure 7). The simulations show a transpiration-dominated pattern in green water fluxes. The most dramatic changes also occurred in Tr with decreases of up to  $13 \pm 6\%$ , especially in the southern forests where a greater proportion of conifer conversion to broadleaves was simulated. Compared to the even-aged scenarios S2B and S2C (Figure 7k,l), uneven-aged scenarios S1B and S1C (Figure 7h,i) had slightly greater impact on reducing catchment-wide Tr. A 50% increase in the proportion of broad-leaved trees focused on the southern conifer forests was projected in a reduction of  $\sim 9 \pm 6\%$  from baseline Tr across the catchment (Figure 7h).

The most marked changes in mean Es were mainly in the southern mixed forest, as the increased cover of deciduous broad-leaved trees allows greater energy inputs to the forest floor in spring prior to leaf-out. Similarly, S1 with younger broad-leaved trees also promoted higher Es due to lower shading (Figure 7m-o).

Ei increased most in even-aged mixed forests, followed by the agroforestry with mature broad-leaved trees (Figure 7v-x). Ei in the uneven-aged mixed forests also declined slightly (Figure 7t,u). ET decreased most in the southern mixed forest, with a small scattered increase at the fringe of the mixed forest, mainly due to increased Es (Figure 7b, c, e,f). For even-aged scenarios (S2A and S2C), ET increased slightly in the formerly arable-dominated northern areas, mainly because the decrease in Tr could not offset the increase in Ei (Figure 7d,f).

Figure 8 shows the differences of modelled blue water fluxes between the stakeholder-designed scenarios and the baseline. Similar to green fluxes, scenarios B and C with mixed forest in the southern catchment showed most marked differences, which were generally greater for the latter. Furthermore, except for infiltration, changes in blue water fluxes were more pronounced for uneven-aged scenarios (S1B and S1C). Ov increased in some places around the stream channels, particularly in the southern mixed forests (Figure 8c). In all

scenarios, Infil slightly decreased following a similar spatial pattern and magnitude to the changes in Ei (Figure 7). However, even the greatest reduction in Infil rates reached only  $\sim 2\%$  of the baseline Infil, which was for the even-aged scenario of replacing conifers with mature broad-leaved trees (Figure 8k). Because of the combined effects of increased ET and decreased Infil, the simulated GWr and GWf were reduced in the northern agroforestry (Figure 8 scenarios A and C). However, despite the slight reduction in Infil, GWr and GWf under mixed forests still increased as the reduction in ET exceeded the reduction in Infil. For coniferous forests, a 50% increase in the proportion of broad-leaved trees was projected to result in an average 11% increase in GWr across the catchment (Figure 8n).

#### 4.4 | Catchment-scale changes in water age

Figure 9 shows the catchment-wide modelled water age changes in streamflow, groundwater, transpiration and soil evaporation. Overall, the spatial patterns of changes were more significant in scenarios B and C; and tended to be greater for the latter. Uniquely, streamwater age showed changes across the whole catchment, meaning upstream land use changes impacted downstream water ages (Figure 9a,d). With the exception of scenarios S2A and S2C, there was a general reduction in streamwater age. Replacement with mature broad-leaved trees in the arable area slightly increased streamwater ages of the whole catchment (Figure 9d,f), whereas impacts of the replacement of conifer forests would be limited within the southern areas as a direct consequence of streamflow direction (Figure 9b,e). Groundwater MRT showed a small increase ( $\sim 0.2$  years) under scenarios with replacement in the arable areas (Figure 9g,j). The turnover of groundwater under mixed forests notably increased, as the groundwater mean residence time was reduced by 2.7–4.4 years ( $\sim 9\%$ – $15\%$  of the baseline) in the original conifer-dominated areas, with the greatest reduction in uneven-aged scenarios (Figure 9h,i). Transpiration water age was projected to generally increase for all scenarios, with S2C demonstrating the highest values. Soil evaporation age was projected to increase for all the scenarios except S2A and S2C where some of the northern arable lands were replaced with mature broad-leaved trees.

#### 4.5 | Land use effects on evapotranspiration and water storage

We also analysed ET losses and groundwater levels at the catchment scale under each land use type and each modelled scenario. Figure 10a shows the long-term average ET rates for each land use type across the entire catchment. Under baseline conditions, arable land—given its extensive coverage—contributed the most to catchment ET. Conifer forests, despite having a more limited spatial extent, had only a slightly lower contribution losses of water in the system than arable lands due to high Tr and Ei rates. In the extreme scenarios, ET losses showed the reverse of effects on streamflow (Figure 6): conifer forests exhibited the highest ET rates, followed by arable

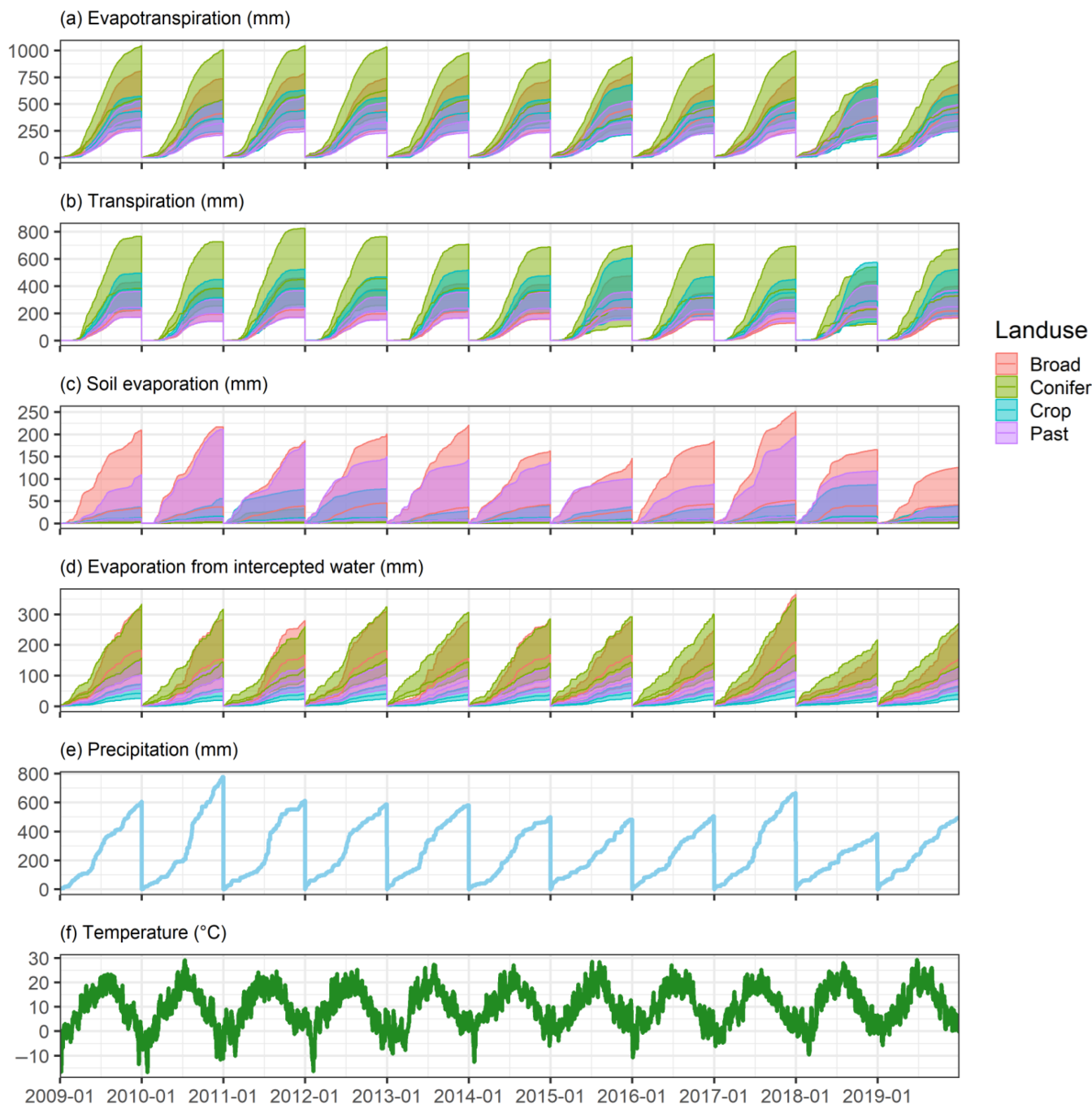


**FIGURE 5** Breakdown of green water fluxes for different land uses: (a) total evapotranspiration, (b) transpiration, (c) soil evaporation and (d) evaporation from intercepted water. (a–e) show the accumulated values for each year, (f) is the daily temperature. Lines represent the simulated median, and shaded regions represent the upper and lower ranges of simulations for the top 10 parameter sets.

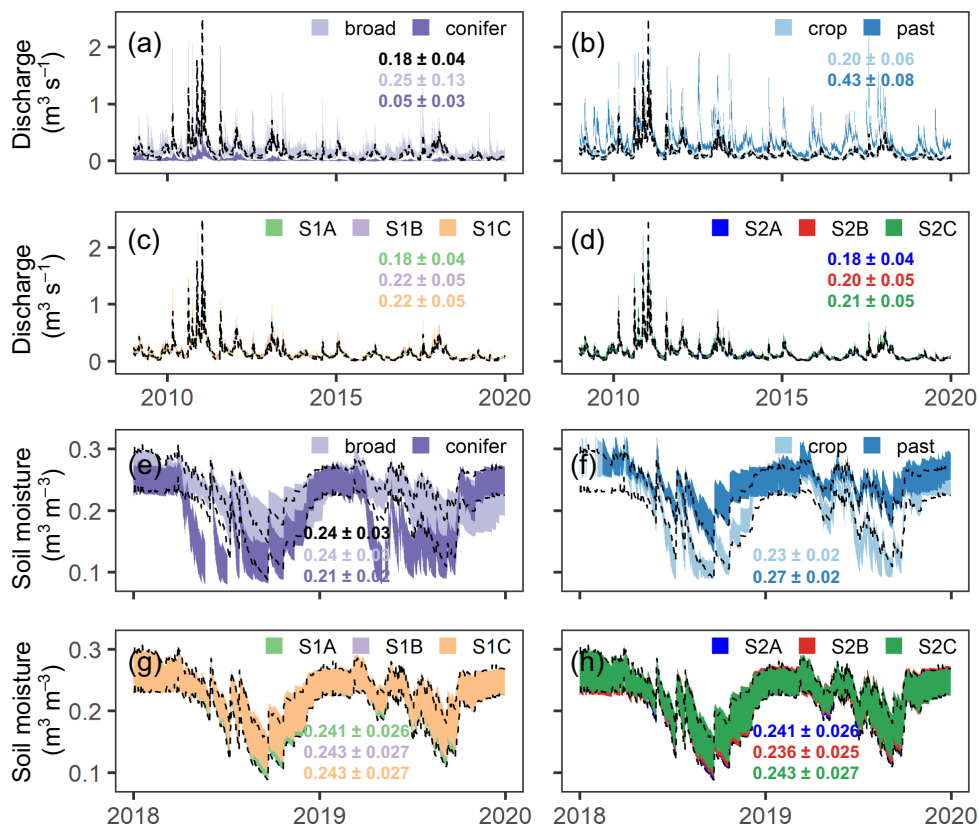
lands, broad-leaved forests and pasture. Among the design scenarios, the most significant differences occurred in the conifer forests in scenarios B and C. The median ET loss of conifer forests dropped by more than 50% in the southern mixed forests. The changes to arable lands were not substantial.

The normalized groundwater level calculated under each land cover (which unlike evapotranspiration rates were not proportionally weighted) were used as a proxy of groundwater storage (Figure 10b). For the

baseline, groundwater storage was highest under arable lands. Meanwhile, in both baseline and extreme scenarios, the groundwater storage under conifer forests was the lowest. Compared to the baseline scenario, the agroforestry scenarios showed no significant change in terms of increasing groundwater storage (S1A and S2A). However, mixed-forest scenarios substantially increased storage in areas where conifer forests were partially replaced; in particular the uneven-aged scenarios almost doubled groundwater storage from baseline (S1B and S1C).



**FIGURE 6** Time series of simulated discharge at Demnitz Mill and soil moisture in the first soil layer (top 15 cm) of the forest site (Figure 1). The area between the two black dashed lines represents the 95% spread of behavioural simulations for the baseline scenario; the shaded areas show the same for the extreme scenarios (a, b, e and f) and designed scenarios (c, d, g and h). The values on the subplots are the long-term (2009–2019) average range of the 95% spread derived from the top 10 parameter sets, the first value being the mean of the simulations over this period. Broad, broad-leaved forest; conifer, conifer forest; crop, arable agricultural land; past, pasture.



## 5 | DISCUSSION

### 5.1 | What is the potential of tracer-aided ecohydrological models in assessing land use effects?

In the face of increased water-related challenges and risks, reliable information for planning water resources is crucial (Vose et al., 2011). Ecohydrological models such as HYLUC (Calder et al., 2003) and RHESSys (Tague & Frew, 2021) have a long history of helping to understand the impact of land use change on water availability in complex landscape systems, and elucidating the relationships between land management, critical zone interactions and water storage-flux dynamics. Such insights can provide an evidence base to help inform policy makers and stakeholders about the potential impacts of different management strategies and their associated uncertainties in regions where water security concerns are growing.

Here, an assessment framework was developed using EcH<sub>2</sub>O-iso to use tracers to help constrain ecohydrological models to evaluate the changing interactions between water, energy and biomass productions across spatio-temporal scales in a lowland drought sensitive catchment under alternative land use scenarios (Figure 3). As in other systems that have been extensively tested and validated under a wide range of climatic and hydrological conditions (Douinot et al., 2019; Knighton et al., 2020; Neill et al., 2021; Smith et al., 2019; Smith, Tetzlaff, Landgraf, et al., 2022; Yang et al., 2021), EcH<sub>2</sub>O-iso was subject to an isotope-aided, spatial distributed, multi-criteria calibration against streamflow, soil moisture, Tr and groundwater (see Figure S2

and S3 and Smith et al. (2021)). This enabled the model to produce robust simulations of water storage-flux-age interactions that could help visualize the spatio-temporal dynamics under contrasting proposed land uses aimed at reducing water losses to the atmosphere and their associated uncertainties.

Previously, reduced uncertainties in process representation have shown that the inclusion of isotopes can increase confidence in the model's simulation of water flux, storage and age dynamics in DMC across a range of hydroclimatic conditions (Smith et al., 2021). This tracer-aided framework provides an integrated modelling approach that can link scales across the catchment and more explicitly constrain storage and age estimates within modelling experiments than conventional modelling without tracers (Xu, & xue, Li, L., & Zhao, J., 2017). The general applicability of the model and its use of increasingly available data to drive it, enhances the transferability of the approach and its potential to be upscaled to larger catchment and regional scales (e.g., Yang et al., 2023).

In applying the framework, we found that both modelled water storage and flux exhibited spatio-temporal variability, which was dominated by the close coupling of land cover type and soil distributions. This provides a powerful tool for demonstrating the crucial role that land management plays in controlling water availability in drought-sensitive landscapes. Such evidence also helps show the potential that land management has to manipulate ecohydrological partitioning and aid regulation of water storage and availability depending on local priorities. The spatial assessments generated by the model provided an intuitive catchment-wide understanding of ecohydrological dynamics

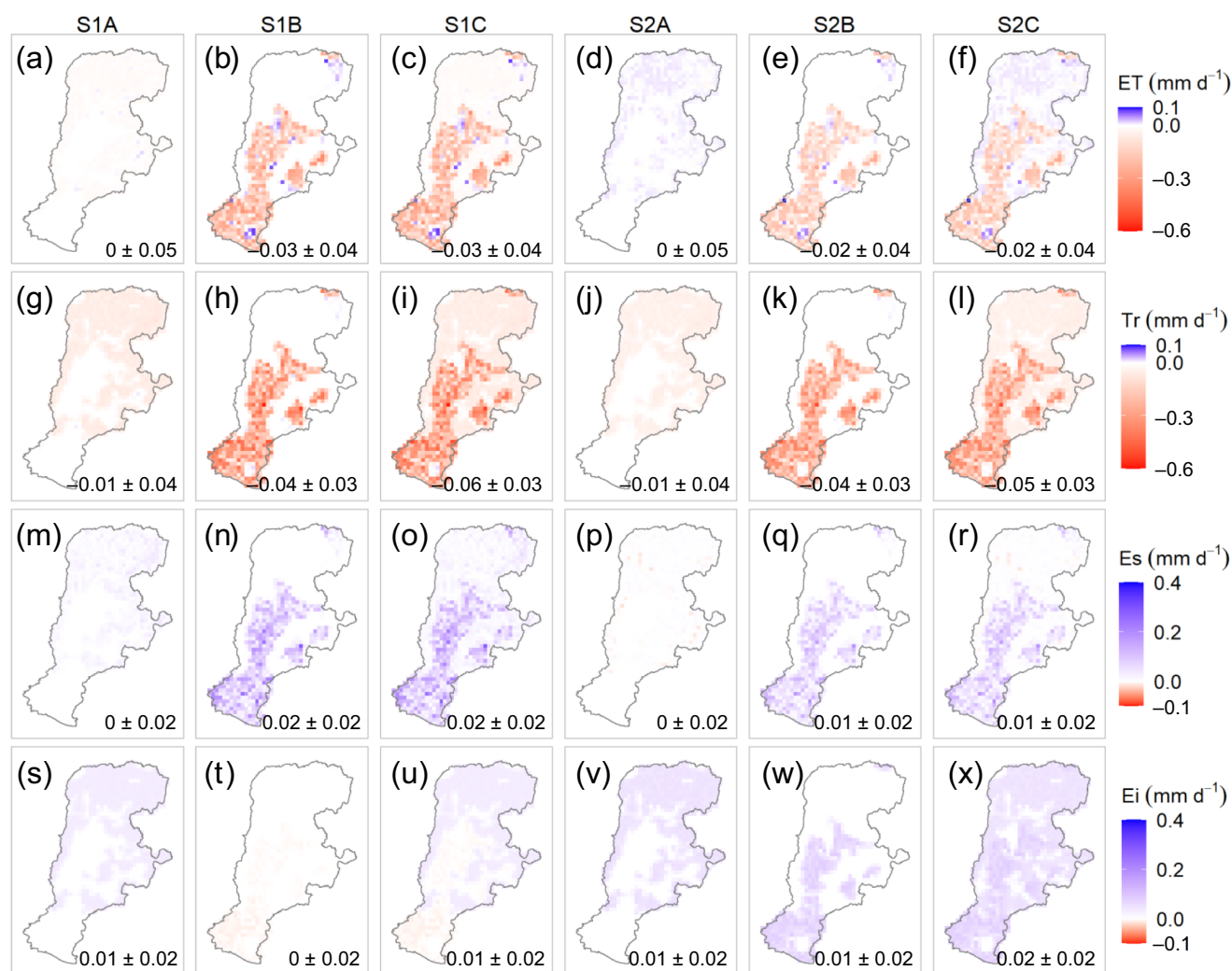


**FIGURE 7** Distribution of differences in long-term (2009–2019) average of daily green fluxes between designed scenarios and baseline. Differences were computed as designed scenarios minus baseline scenario. The values shown on the subplots are catchment-wide, long-term (2009–2019) average and standard deviations. Ei, evaporation from intercepted water; Es, soil evaporation; ET, total evapotranspiration; Tr, transpiration.

that can aid communication with and between stakeholders. For example, the model showed that conifer monocultures have higher ET and lower GWR compared with other land covers (Figure 4) consistent with previous research in the same region (Douinot et al., 2019) and other temperate landscapes (e.g., Calder et al., 2003). Furthermore, the temporal results highlight the cascading effects of land management on stream-flow generation, and the most marked impacts on low flow periods (Figure 6 and Table S3). With associated representation of model uncertainty, such outputs can be an important part of the evidence base and decision support tools for developing policies for land and water management in such drought-sensitive landscapes (Ahn & Merwade, 2017; Calder, 2005; Delgado et al., 2010). Moreover, by examining time series simulations, we can zoom in on specific stress periods or locations and gain a more nuanced understanding of the non-linear effects of land management on water storage and flux under different hydroclimatic periods (Smith, Tetzlaff, Maneta, & Soulsby, 2022a).

## 5.2 | How do land use changes affect green and blue water flux partitioning?

Land use type and extent are a first order control on water partitioning with a given area, and quantifying the implications for water availability are fundamental to development of sustainable policies and planning (Ahn & Merwade, 2017). Using generic land use types in DMC, annual water use generally increases in the order of pasture (median ET 340 mm a<sup>-1</sup>) < crops (400 mm a<sup>-1</sup>) < broadleaved trees (432 mm a<sup>-1</sup>) < conifers (510 mm a<sup>-1</sup>) with increased interception being the dominant flux of increased water loss under forest canopies (Table S2). Thus changes such as diversifying conifer forests with broadleaves or converting agricultural land to agroforestry, alter the amount of water intercepted by vegetation (Figure 7s–x). Although these changes in Ei might appear subtle, a change of 0.01 from a baseline of 0.11 represents a relative change of roughly 9%. In scenarios

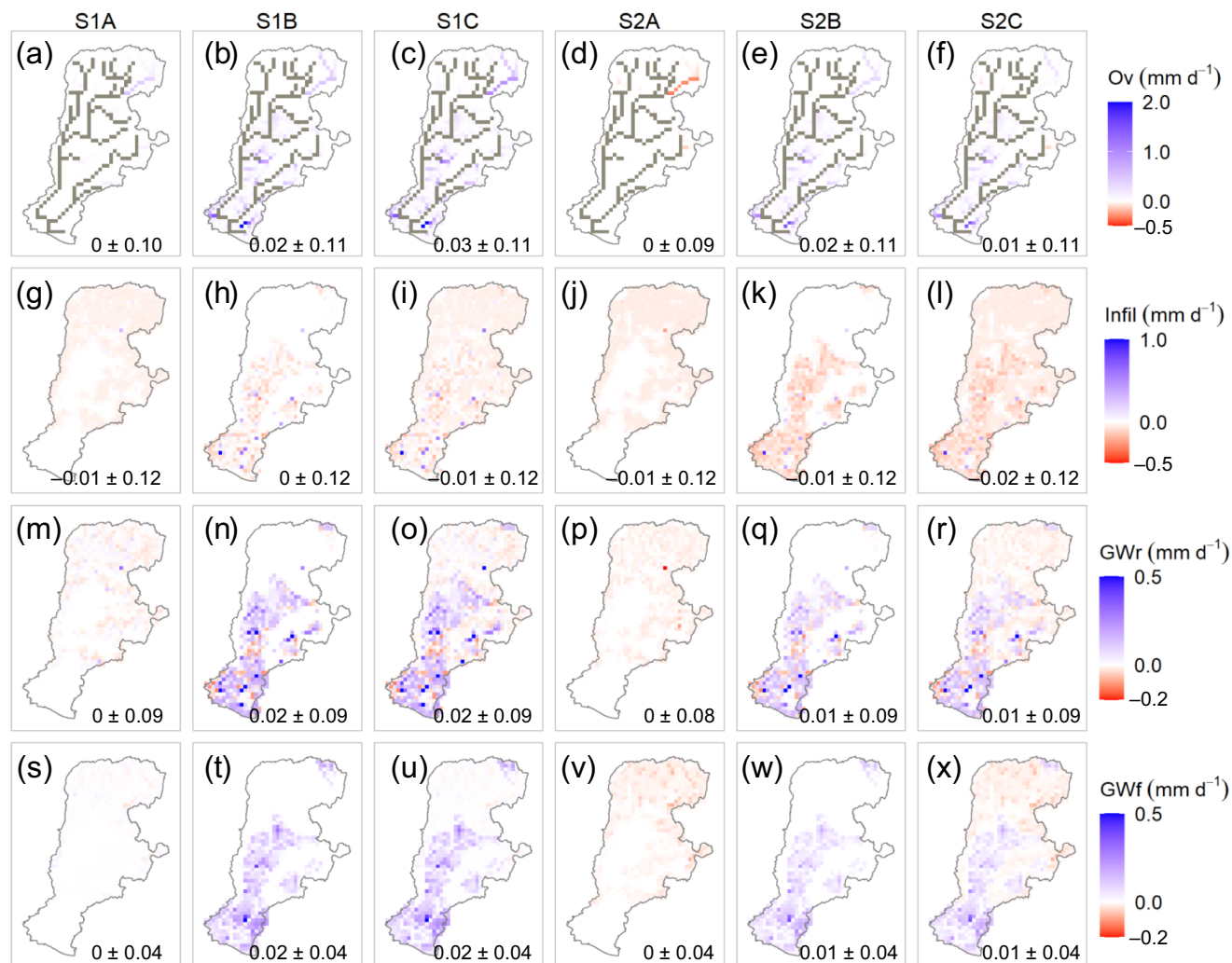


**FIGURE 8** Distribution of differences in long-term (2009–2019) average of daily blue fluxes between designed scenarios and baseline. Differences are computed as designed scenarios minus baseline scenario. The grey cells on the overland flow sub-figure indicate stream paths without simulated overland flow. The values shown on the subplots are catchment-wide, long-term (2009–2019) average and standard deviations. GWf, cell-to-cell lateral groundwater flow; GWr, groundwater recharge; Infil, infiltration into the first soil layer (L1, top 15 cm); Ov, cell-to-cell overland flow.

like S2C, the relative change reaches nearly 18%. Such variations, even if they seem relatively small in absolute terms, can cumulatively impact the amount of water available for transpiration and ultimately affect the amount of blue water that can be recharged into subsurface storage or streams (Figure 8).

Furthermore, land use changes can alter vegetation composition and different plant types that have different water use strategies depending upon their physiology. These changes, which can be parameterised in the model (e.g., LAI, canopy storage, stomatal conductance, rooting distributions—see Table S1), can affect water partitioning. Modelling in DMC indicated that conifer forests, despite their smaller area, have only slightly lower contributions to total catchment ET losses compared with the dominant arable lands as a result of greater interception loss and their high  $Tr$  rates (Figure 10). This aligns with previous findings in central Europe (Calder et al., 2003; Cannell, 1999). However, after implementation of design

scenarios, the simulated total green fluxes markedly dropped in the mixed forests, particularly in terms of  $Tr$  as  $Ei$  remained high and  $Es$  increased (Figure 7). This resulted in an increase in GWr and GWf (Figure 8). A recent study used a European tree-ring database to show that mixed forests, particularly of conifers and broadleaves, are more resilient to drought. This may point to multiple advantages in forest management adopting more nature-based solutions based on more diverse species composition and lower planting densities (Pardos et al., 2021).

Simulations also showed that uneven-aged management of conifer and young broad-leaved forests could further reduce catchment ET and increase recharge (Figures 7 and 8). This aligns with more traditional selection silviculture, which creates and maintains uneven-aged forest structures through selective felling of individual trees or small groups of trees to maintain more sustainable regeneration (Brüllhardt et al., 2022; Nyland, 2016). These findings demonstrate

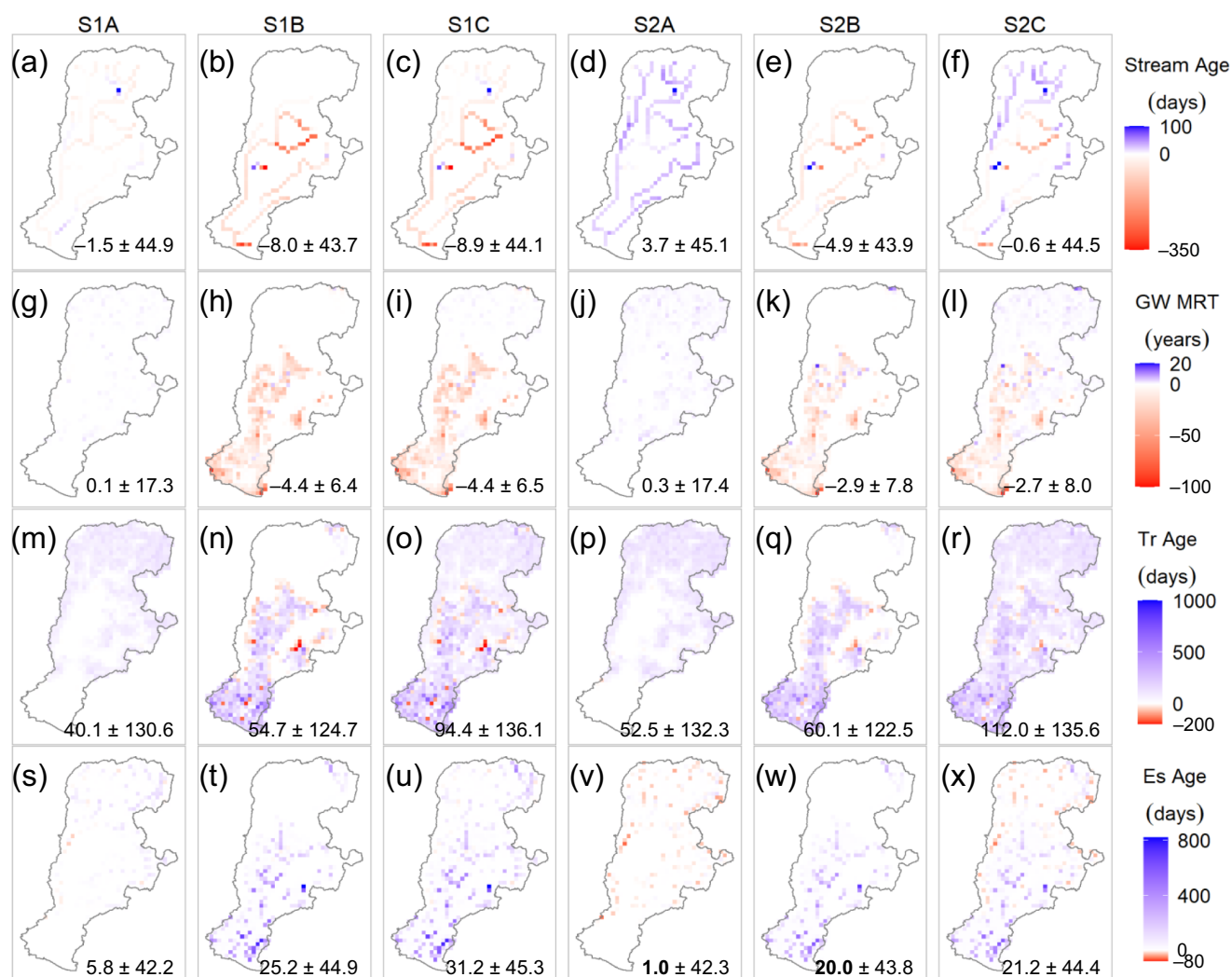


**FIGURE 9** Distribution of differences in long-term (2009–2019) average of water ages between designed scenarios and baseline. Differences were computed as designed scenarios minus baseline scenario. Stream age, streamwater age; GW MRT, groundwater mean residence time; Tr age, transpiration water age; Es age, soil evaporation water age.

the potential benefits and strong influence of active management, as well as generic land cover type, in manipulating ecohydrological partitioning in a more sustainable way.

### 5.3 | What are the implications for water storage and age?

Quantifying water storage dynamics is critical for improving understanding of water cycling (Zhou et al., 2022) and regulating water partitioning in terrestrial ecohydrological systems (Bouaziz et al., 2020). In this regard, tracer-aided models calibrated against extensive isotopic data can better constrain the subsurface storage needed to explain tracer damping and mixing (Soulsby et al., 2015). Catchment water storage can be indexed by soil moisture and groundwater storage. Infiltration and recharge are important processes for increasing water storage, whereas ET is the main exit route of water from the

catchment. Here, soil moisture under extreme conifer forests and arable lands were similar and lower than in other scenarios, particularly during the growing season when coniferous trees and crops account for large water losses (Figure 6e) indicating the potential vulnerability of these land uses in terms of drought resilience.

Under agroforestry, no major changes were simulated in terms of increasing groundwater storage in the catchment (Figure 10b) reflecting the increased tree cover leading to higher levels of ET due to increased interception and reduced infiltration, though the limited extent of the increased tree cover (10%) dictated that modelled effects were small. This is consistent with recent similar eddy covariance measurements of ET over crops and agroforestry at several sites in Germany (Markwitz et al., 2020). However, mixed-forest scenarios increased storage when replacing conifer forests; with the uneven-aged scenarios almost doubling the groundwater storage in the modelled domain compared to baseline (Figure 10b). This emphasizes the importance of management decisions on species selection and age in



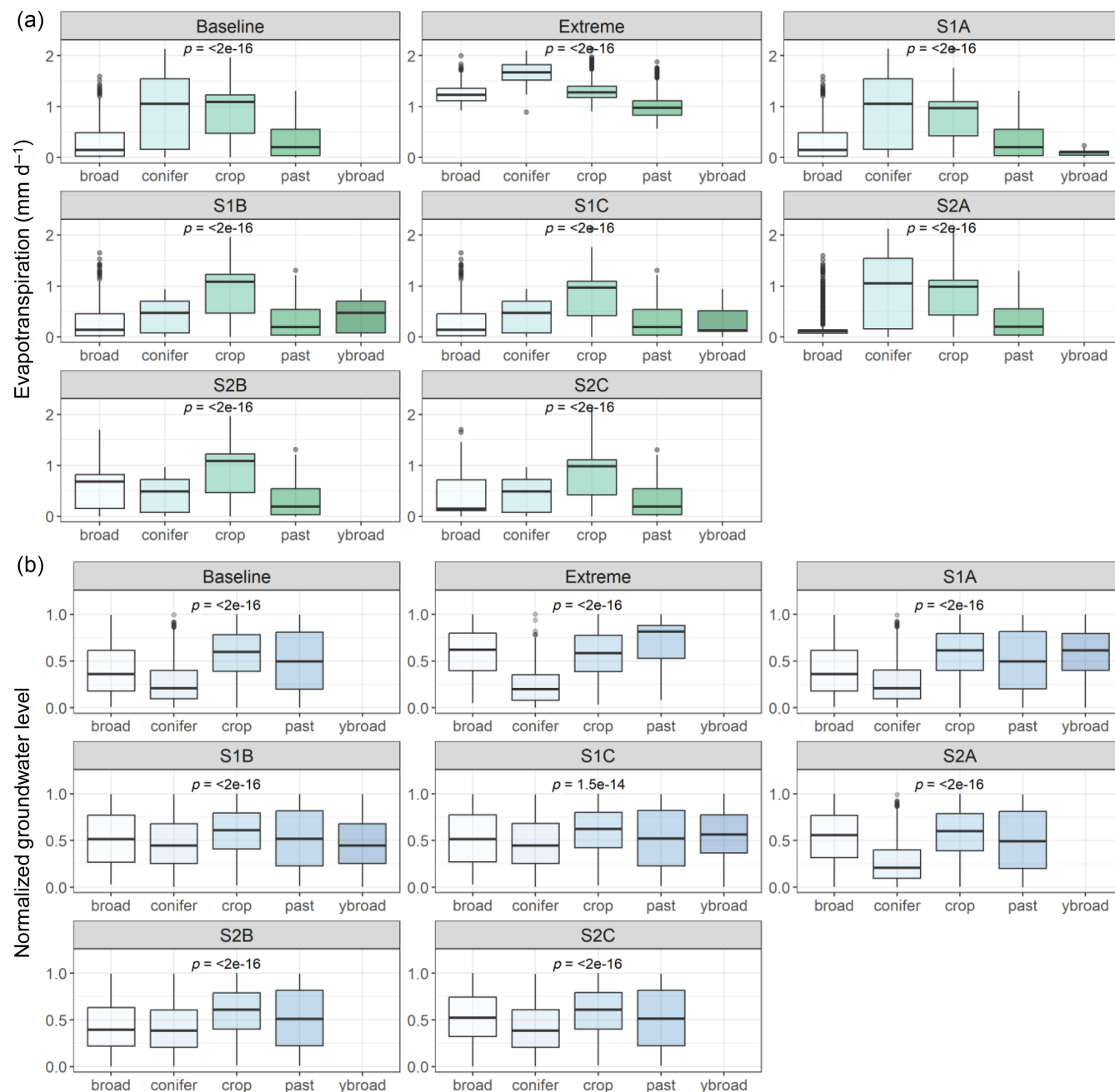


**FIGURE 10** Boxplot of estimated average catchment (a) evapotranspiration contribution and (b) normalized groundwater levels (as a proxy of groundwater storage) for land use types of broad-leaved forest (broad), conifer forest (conifer), croplands (crop), pasture (past) and young broadleaved forest (ybroad) under different scenarios. The lower/upper box boundaries are the 25th/75th percentiles, respectively, the inner box line is the median, and the lower/upper error lines are the 10th/90th percentiles, respectively. Note that the evapotranspiration is proportional to cellwise land cover, and the groundwater storage was computed as the groundwater level under certain land cover. The  $p$ -values represent that the differences between the means of different land use types were statistically significant ( $p < 2e-16$  denotes value close to 0).

manipulating catchment water storage and improving water availability, water uptake, or water use efficiency. Further, management has to be compatible with local climatic and edaphic conditions (Pardos et al., 2021).

Quantifying the ages of water through tracer-aided ecohydrological models can also provide valuable insights into the impact of land use change on the interactions between water fluxes and storage

within landscapes (Sprenger et al., 2019). Although uncertain, simulations showed that the inclusion of broad-leaved trees in mixed forests could increase the turnover of groundwater (Figure 9) as increased recharge can help accelerate the movement of water in the subsurface (Befus et al., 2017). This can reduce recovery times from external disturbances such as drought and thus, enhance landscape resilience (Griebler & Avramov, 2015; Smith, Tetzlaff, Maneta, & Soulsby, 2022a).

## 5.4 | Towards more drought-resilient land management?

The modelling presented here is a first step towards providing a learning framework for understanding how land use change might be used to manage water cycling and availability in the DMC. Although this already provides evidence that can aid decision making, further improving understanding will depend on integrating insights from other studies, new data and thinking how to refine the modelling further. Fundamental to this will be embedding stakeholders more strongly into the modelling work flow to ensure that results can most usefully contribute to more resilient decision making given the likelihood of a warmer, drier future for DMC.

For example, there is growing evidence showing benefits of agroforestry in enhancing water storage and soil moisture, and thus, increasing drought resilience (Kuyah et al., 2019; Siriri et al., 2013). However, each situation is complex with a different geographical context; thus, more optimal water use through agroforestry cannot be generalized for all systems (Bayala & Prieto, 2020). In DMC, for example, modelling showed that the combination of increased ET and decreased infiltration can lead to slightly reduced groundwater recharge and groundwater flow in agroforestry (Figure 8 scenarios A and C). Although this does not diminish the potential of agroforestry in terms of maintaining soil moisture, it highlights the trade-offs of affecting different ecosystem services. Ecohydrological modelling can be parameterized to capture more specific variations within generic land use types (e.g., species-specific traits, tree-crop ratios etc. in agroforestry) and can be used to explore the potential impacts of agroforestry or other land uses in more detail (Liu et al., 2018). Now that field data are becoming available from eddy covariance (e.g., Markwitz et al., 2020) or isotope data (Landgraf et al., 2023), there is the potential for further model testing and refinement.

The potential for diverse, uneven-age mixed forests for improving drought resilience was highlighted by the simulations. Even in the dry year, groundwater recharge and streamflow generation were predicted to be enhanced under mixed-forest with uneven-aged management (Figure S6 and S7). Other benefits of mixed-forest management have been reported elsewhere (Felton et al., 2010, 2016; Liu et al., 2018), including increased biodiversity, reduced stand vulnerability to pest damage, increased bird abundance and so forth. (Alder et al., 2018; Felton et al., 2016). The modelling approach in DMC offers an efficient and transferable tool to investigate, visualize and communicate spatio-temporal effects and inherent uncertainties of a wide range of management strategies in building drought resilience (Pardos et al., 2021). Moreover, the model has the potential to go beyond the “snap shot” assessment of alternative management strategies in time, modelling forest growth dynamics over shorter timesteps and including climate change scenarios in addition to land use change (Douinot et al., 2019; Kuppel et al., 2018; Maneta & Silverman, 2013).

The EcH<sub>2</sub>O-iso application here involved relatively simple representation of land cover manipulations as a first step in the assessment of land use impacts on ecohydrological partitioning. More detailed analysis is possible but would require: (a) further data collection,

(b) model improvements and (c) even more direct stakeholder engagement in understanding model outputs and uncertainty. In terms of data, the model calibration showed the value of soil isotope data and transpiration proxies (sap flux rates) in constraining the model. For more detailed applications for different species, ages, densities, management options, additional data on LAI changes, interception losses, rooting distributions would likely prove effective calibration constraints. For model improvements, the land use change impacts are currently largely assessed via structural changes to the vegetation (cf. Neill et al., 2021). However, EcH<sub>2</sub>O-iso allows vegetation dynamics to be assessed (Douinot et al., 2019), and temporal changes in soil properties associated with land use change need to be incorporated (e.g., Poorter et al., 2021). In this regard, recent forest productivity changes associated with drought conditions could be used to better understand the complex lag effects of droughts on forests physiology and water cycling and incorporate this behaviour in models (e.g., Pohl et al., 2023).

Furthermore, the limitations associated with calibration through random sampling can be possibly mitigated by implementing more structured calibration methods, such as formal Bayesian DREAM approach (Vrugt et al., 2009) and Limits of Acceptability framework (Beven, 2019) though this would result in significantly higher computation time. Finally, although the modelling outputs give intuitive insights into the likely spatio-temporal impacts of land use change options (Smith, Tetzlaff, Maneta, & Soulsby, 2022b), the results are uncertain and ensuring effective stakeholder communication and understanding of this is a key priority.

## 6 | CONCLUSION

We developed a framework for quantifying and visualizing the impact of different land use management strategies on water flux partitioning, storage and age. This utilizes the novel spatially-distributed and tracer-aided ecohydrological model, EcH<sub>2</sub>O-iso, to analyse extreme and plausible design scenarios and consider uncertainties. Using modelling experiments to examine the effects of diversification and introduce broadleaved trees into arable and coniferous monocultures, we found that uneven-aged mixed forests of conifer and broadleaved trees had the greatest potential to impact on increasing water availability in the catchment. Agroforestry showed no significant changes in groundwater storage, likely due to the limited tree cover extent (~10%) used in the scenario. We demonstrated the potential benefits and influence of active management, as well as the importance of generic land cover type, in manipulating ecohydrological partitioning in a more sustainable way. Our results underscore the importance of further developing ecohydrological modelling and integrating more empirical data to improve understanding of how land management can manipulate water availability to build drought resilience at contrasting temporal and spatial scales. Beyond providing insights from a hydrological perspective, our study offers valuable knowledge to help make scientifically informed decisions regarding optimal land use changes. The findings should encourage stakeholders to consider

strategic diversification towards uneven-aged mixed forests, given their potential in enhancing drought resilience.


## ACKNOWLEDGEMENTS

Funding was received through the Einstein Research Unit “Climate and Water under Change” from the Einstein Foundation Berlin and Berlin University Alliance (grant no. ERU-2020-609). We acknowledge the use of computational resources of the Climate Geography group of Humboldt-Universität zu Berlin. We also thank Songjun Wu for his support in setting up the HPC and colleagues from the Finck Foundation ([www.finck-stiftung.org](http://www.finck-stiftung.org)) Benedict Boesel and Max Kuester for the trustful collaboration, for providing study site access and their insight knowledge on reasonable and plausible land use scenarios. Contributions from CS were supported by the Leverhulme Trust through the ISO-LAND project (grant no. RPG 2018 375). Open Access funding enabled and organized by Projekt DEAL.

## DATA AVAILABILITY STATEMENT

The data that support the findings of this study are available at (German Meteorological Service, 2020; Myneni et al., 2015; Running et al., 2017; Smith et al., 2021). The model code of EcH<sub>2</sub>O-iso is publicly available at [http://bitbucket.igb-berlin.de:7990/users/ech2o/repos/ech2o\\_iso/browse](http://bitbucket.igb-berlin.de:7990/users/ech2o/repos/ech2o_iso/browse) (last access: Dec 2022).

## ORCID

Shuxin Luo  <https://orcid.org/0000-0002-9876-8872>  
Chris Soulsby  <https://orcid.org/0000-0001-6910-2118>

## REFERENCES

- Ahn, K. H., & Merwade, V. (2017). The effect of land cover change on duration and severity of high and low flows. *Hydrological Processes*, 31(1), 133–149. <https://doi.org/10.1002/hyp.10981>
- Alder, D. C., Fuller, R. J., & Marsden, S. J. (2018). Implications of transformation to irregular silviculture for woodland birds: A stand wise comparison in an English broadleaf woodland. *Forest Ecology and Management*, 422, 69–78.
- Astrup, R., Bernier, P. Y., Genet, H., Lutz, D. A., & Bright, R. M. (2018). A sensible climate solution for the boreal forest. *Nature Climate Change*, 8(1), 11–12.
- Bayala, J., & Prieto, I. (2020). Water acquisition, sharing and redistribution by roots: Applications to agroforestry systems. *Plant and Soil*, 453(1–2), 17–28. <https://doi.org/10.1007/s11104-019-04173-z>
- Befus, K. M., Jasechko, S., Luijendijk, E., Gleeson, T., & Bayani Cardenas, M. (2017). The rapid yet uneven turnover of Earth's groundwater. *Geophysical Research Letters*, 44(11), 5511–5520.
- Beven, K. (2019). Towards a methodology for testing models as hypotheses in the inexact sciences. *Proceedings of the Royal Society A*, 475(2224), 20180862.
- Birkel, C., Soulsby, C., & Teztlaff, D. (2011). Estimating catchment scale water storage dynamics: Reconciling contrasting insights from rainfall-runoff models and tracers. *Hydrological Processes*, 25, 3924–3936.
- Bogucki, P. (1996). The spread of early farming in Europe. *American Scientist*, 84(3), 242–253.
- Böse, M., & Brande, A. (2010). Landscape history and man-induced landscape changes in the young morainic area of the north European plain—A case study from the Bäke Valley, Berlin. *Geomorphology*, 122(3–4), 274–282.
- Bouaziz, L. J. E., Steele-Dunne, S. C., Schellekens, J., Weerts, A. H., Stam, J., Sprockereef, E., Winsemius, H. H. C., Savenije, H. H. G., & Hrachowitz, M. (2020). Improved understanding of the link between catchment-scale vegetation accessible storage and satellite-derived soil water index. *Water Resources Research*, 56(3), 1–22. <https://doi.org/10.1029/2019WR026365>
- Brüllhardt, M., Rotach, P., Forrester, D. I., & Bugmann, H. (2022). Sustainable regeneration in uneven-aged mixed deciduous forests managed by selection silviculture: The role of demographic structure. *Forestry*, 95(2), 201–214.
- Calder, I. R. (2005). *Blue revolution—Integrated land and water resources management* London. UK.
- Calder, I. R., Reid, I., Nisbet, T. R., & Green, J. C. (2003). Impact of lowland forests in England on water resources: Application of the hydrological land use change (HYLUC) model. *Water Resources Research*, 39(11), 1319–1329.
- Cannell, M. G. R. (1999). Environmental impacts of forest monocultures: Water use, acidification, wildlife conservation, and carbon storage. In *Planted forests: Contributions to the quest for sustainable societies* (pp. 239–262). Springer.
- Craig, H., & Gordon, L. I. (1965). Deuterium and oxygen 18 variations in the ocean and the marine atmosphere.
- De Groot, G. S., Aizen, M. A., Sáez, A., & Morales, C. L. (2021). Large-scale monoculture reduces honey yield: The case of soybean expansion in Argentina. *Agriculture, Ecosystems and Environment*, 306(August 2020), 107203. <https://doi.org/10.1016/j.agee.2020.107203>
- Delgado, J., Llorens, P., Nord, G., Calder, I. R., & Gallart, F. (2010). Modelling the hydrological response of a Mediterranean medium-sized headwater basin subject to land cover change: The Cardener River basin (NE Spain). *Journal of Hydrology*, 383(1–2), 125–134.
- Douinot, A., Tetzlaff, D., Maneta, M., Kuppel, S., Schulte-Bisping, H., & Soulsby, C. (2019). Ecohydrological modelling with EcH<sub>2</sub>O-iso to quantify forest and grassland effects on water partitioning and flux ages. *Hydrological Processes*, 33(16), 2174–2191. <https://doi.org/10.1002/hyp.13480>
- Estrela, T., & Vargas, E. (2012). Drought management plans in the European Union. The case of Spain. *Water Resources Management*, 26(6), 1537–1553.
- Fatichi, S., Pappas, C., & Ivanov, V. Y. (2016). Modeling plant–water interactions: An ecohydrological overview from the cell to the global scale. *Wiley Interdisciplinary Reviews: Water*, 3(3), 327–368. <https://doi.org/10.1002/wat2.1125>
- Felton, A., Lindbladh, M., Brunet, J., & Fritz, Ö. (2010). Replacing coniferous monocultures with mixed-species production stands: An assessment of the potential benefits for forest biodiversity in northern Europe. *Forest Ecology and Management*, 260(6), 939–947. <https://doi.org/10.1016/j.foreco.2010.06.011>
- Felton, A., Nilsson, U., Sonesson, J., Felton, A. M., Roberge, J. M., Ranius, T., Ahlström, M., Bergh, J., Björkman, C., Boberg, J., Drössler, L., Fahlvik, N., Gong, P., Holmström, E., Keskitalo, E. C. H., Klapwijk, M. J., Laudon, H., Lundmark, T., Niklasson, M., ... Wallertz, K. (2016). Replacing monocultures with mixed-species stands: Ecosystem service implications of two production forest alternatives in Sweden. *Ambio*, 45, 124–139. <https://doi.org/10.1007/s13280-015-0749-2>
- Gat, J. R. (1995). Stable isotopes of fresh and saline lakes. In *Physics and chemistry of lakes* (pp. 139–165). Springer.
- Gelbrecht, J., Fait, M., Dittrich, M., & Steinberg, C. (1998). Use of GC and equilibrium calculations of CO<sub>2</sub> saturation index to indicate whether freshwater bodies in north-eastern Germany are net sources or sinks for atmospheric CO<sub>2</sub>. *Fresenius' Journal of Analytical Chemistry*, 361(1), 47–53.
- Gelbrecht, J., Lengsfeld, H., Pöthig, R., & Opitz, D. (2005). Temporal and spatial variation of phosphorus input, retention and loss in a small catchment of NE Germany. *Journal of Hydrology*, 304(1–4), 151–165.

- German Meteorological Service. (2020). Climate data center [Dataset]. Retrieved from <https://cdc.dwd.de/portal/shortlink/fa4185e9-1171-470b-8e04-16f122095167>
- Griebler, C., & Avramov, M. (2015). Groundwater ecosystem services: A review. *Freshwater Science*, 34(1), 355–367. <https://doi.org/10.1086/679903>
- Grillakis, M. G. (2019). Increase in severe and extreme soil moisture droughts for Europe under climate change. *Science of the Total Environment*, 660, 1245–1255.
- Gu, C., Ma, J., Zhu, G., Yang, H., Zhang, K., Wang, Y., & Gu, C. (2018). Partitioning evapotranspiration using an optimized satellite-based ET model across biomes. *Agricultural and Forest Meteorology*, 259(July 2017), 355–363. <https://doi.org/10.1016/j.agrformet.2018.05.023>
- Guswa, A. J., Tetzlaff, D., Selker, J. S., Carlyle-Moses, D. E., Boyer, E. W., Bruen, M., Cayuela, C., Creed, I. F., Van de Giesen, N., Grasso, D., Hannah, D. M., Hudson, J. E., Hudson, S. A., Iida, S., Jackson, R. B., Katul, G. G., Kumagai, T., Llorens, P., Lopes Ribeiro, F., ... Levía, D. F. (2020). Advancing ecohydrology in the 21st century: A convergence of opportunities. *Ecohydrology*, 13(4), 1–14. <https://doi.org/10.1002/eco.2208>
- Hrachowitz, M., Savenije, H., Bogaard, T. A., Tetzlaff, D., & Soulsby, C. (2013). What can flux tracking teach us about water age distribution patterns and their temporal dynamics? *Hydrology and Earth System Sciences*, 17(2), 533–564.
- Jarvis, P. G. (1976). The interpretation of the variations in leaf water potential and stomatal conductance found in canopies in the field. *Philosophical Transactions of the Royal Society of London. B, Biological Sciences*, 273(927), 593–610.
- Johann, E. (2006). *Historical development of nature-based forestry in Central Europe*. Nature-based forestry in Central Europe.
- Jones, A., Panagos, P., Barcelo, S., Bouraoui, F., Bosco, C., Dewitte, O., Gardi, C., Erhard, M., Hervás, J., Hiederer, R., Jeffery, S., Lükewille, A., Marmo, L., Montanarella, L., Olazábal, C., Petersen, J.-E., Penizek, V., Strassburger, T., Tóth, G., ... Yigini, Y. (2012). The state of soil in Europe. *JRC Reference Reports*, 78, 25186.
- Kleine, L., Tetzlaff, D., Smith, A., Dubbert, M., & Soulsby, C. (2021). Modeling ecohydrological feedbacks in forest and grassland plots under a prolonged drought anomaly in central Europe 2018–2020. *Hydrological Processes*, 35(8), e14325.
- Knighton, J., Kuppel, S., Smith, A., Soulsby, C., Sprenger, M., & Tetzlaff, D. (2020). Using isotopes to incorporate tree water storage and mixing dynamics into a distributed ecohydrologic modelling framework. *Ecohydrology*, 13(3), e2201. <https://doi.org/10.1002/eco.2201>
- Kowalski, K., Okujeni, A., Brell, M., & Hostert, P. (2022). Quantifying drought effects in central European grasslands through regression-based unmixing of intra-annual Sentinel-2 time series. *Remote Sensing of Environment*, 268, 112781. <https://doi.org/10.1016/j.rse.2021.112781>
- Kuppel, S., Tetzlaff, D., Maneta, M. P., & Soulsby, C. (2018). Ech2O-iso 1.0: Water isotopes and age tracking in a process-based, distributed ecohydrological model. *Geoscientific Model Development*, 11(7), 3045–3069.
- Kuppel, S., Tetzlaff, D., Maneta, M. P., & Soulsby, C. (2020). Critical zone storage controls on the water ages of ecohydrological outputs. *Geophysical Research Letters*, 47(16), e2020GL088897.
- Kuuluvainen, T., & Gauthier, S. (2018). Young and old forest in the boreal: Critical stages of ecosystem dynamics and management under global change. *Forest Ecosystems*, 5(1), 1–15. <https://doi.org/10.1186/s40663-018-0142-2>
- Kuyah, S., Whitney, C. W., Jonsson, M., Sileshi, G. W., Öborn, I., Muthuri, C. W., & Luedeling, E. (2019). Agroforestry delivers a win-win solution for ecosystem services in sub-Saharan Africa. A meta-analysis. *Agronomy for Sustainable Development*, 39(5), 1–18. <https://doi.org/10.1007/s13593-019-0589-8>
- Landgraf, J., Tetzlaff, D., Birkel, C., Stevenson, J. L., & Soulsby, C. (2023). Assessing land use effects on ecohydrological partitioning in the critical zone through isotope-aided modelling. *Earth Surface Processes and Landforms*, 48, 3199–3219.
- Liu, C. L. C., Kuchma, O., & Krutovsky, K. V. (2018). Mixed-species versus monocultures in plantation forestry: Development, benefits, ecosystem services and perspectives for the future. *Global Ecology and Conservation*, 15, e00419. <https://doi.org/10.1016/j.gecco.2018.e00419>
- Maneta, M. P., & Silverman, N. L. (2013). A spatially distributed model to simulate water, energy, and vegetation dynamics using information from regional climate models. *Earth Interactions*, 17(11), 1–44.
- Markwitz, C., Knohl, A., & Siebicke, L. (2020). Evapotranspiration over agroforestry sites in Germany. *Biogeosciences*, 17(20), 5183–5208.
- Massmann, G., Sültenfuß, J., & Pekdeger, A. (2009). Analysis of long-term dispersion in a river-recharged aquifer using tritium/helium data. *Water Resources Research*, 45(2), W02431.
- MLUK-Ministerium für Landwirtschaft, U. und K. (2021). Low water concept in Brandenburg State. Retrieved from <https://mluk.brandenburg.de/sixcms/media.php/9/Landesniedrigwasserkonzept-Brandenburg.pdf>
- Morris, M. D. (1991). Factorial sampling plans for preliminary computational experiments. *Technometrics*, 33(2), 161–174.
- Myneni, R., Knyazikhin, Y., & Park, T. (2015). MOD15A2H MODIS/Terra leaf area index/FPAR 8-day L4 global 500m SIN grid V006 [dataset]. NASA EOSDIS Land Processes DAAC. <https://doi.org/10.5067/MODIS/MOD15A2H.006>
- Nash, J. E., & Sutcliffe, J. V. (1970). River flow forecasting through conceptual models part I—A discussion of principles. *Journal of Hydrology*, 10(3), 282–290.
- Neill, A. J., Birkel, C., Maneta, M. P., Tetzlaff, D., & Soulsby, C. (2021). Structural changes to forests during regeneration affect water flux partitioning, water ages and hydrological connectivity: Insights from tracer-aided ecohydrological modelling. *Hydrology and Earth System Sciences*, 25(9), 4861–4886. <https://doi.org/10.5194/hess-25-4861-2021>
- Nyland, R. D. (2016). *Silviculture: Concepts and applications*. Waveland Press.
- Pardos, M., Del Río, M., Pretzsch, H., Jactel, H., Bielak, K., Bravo, F., Brazaitis, G., Defosse, E., Engel, M., Godvot, K., Jacobs, K., Jansone, L., Jansons, A., Morin, X., Nothdurft, A., Oreti, L., Ponette, Q., Pach, M., Riofrio, J., ... Calama, R. (2021). The greater resilience of mixed forests to drought mainly depends on their composition: Analysis along a climate gradient across Europe. *Forest Ecology and Management*, 481(September 2020), 118687. <https://doi.org/10.1016/j.foreco.2020.118687>
- Pohl, F., Werban, U., Kumar, R., Hildebrandt, A., & Rebmann, C. (2023). Observational evidence of legacy effects of the 2018 drought on a mixed deciduous forest in Germany. *Scientific Reports*, 13(1), 10863.
- Poorter, L., Craven, D., Jakovac, C. C., Van Der Sande, M. T., Amissh, L., Bongers, F., Chazdon, R. L., Farrior, C. E., Kambach, S., Meave, J. A., Muñoz, R., Norden, N., Rüger, N., Van Breugel, M., Zambrano, A. M. A., Amani, B., Andrade, J. L., Brancalion, P. H. S., Broadbent, E. N., ... Hérault, B. (2021). Multidimensional tropical forest recovery. *Science*, 374(6573), 1370–1376.
- Running, S., Mu, Q., & Zhao, M. (2017). MOD16A2 MODIS/Terra net evapotranspiration 8-day L4 global 500m SIN grid V006 [dataset]. NASA EOSDIS Land Processes DAAC. <https://doi.org/10.5067/MODIS/MOD16A2.006>
- Savilaakso, S., Johansson, A., Häkkinen, M., Uusitalo, A., Sandgren, T., Mönkkönen, M., & Puttonen, P. (2021). What are the effects of even-aged and uneven-aged forest management on boreal forest biodiversity in Fennoscandia and European Russia? A systematic review. *Environmental Evidence*, 10(1), 1–38. <https://doi.org/10.1186/s13750-020-00215-7>



- Schuld, B., Buras, A., Arend, M., Vitas, Y., Beierkuhnlein, C., Damm, A., Gharun, M., Grams, T. E. E., Hauck, M., Hajek, P., Hartmann, H., Hiltbrunner, E., Hoch, G., Holloway-Phillips, M., Körner, C., Larysch, E., Lübke, T., Nelson, D. B., Rammig, A., ... Kahmen, A. (2020). A first assessment of the impact of the extreme 2018 summer drought on central European forests. *Basic and Applied Ecology*, 45, 86–103. <https://doi.org/10.1016/j.baae.2020.04.003>
- Schwaab, J., Davin, E. L., Bebi, P., Duguay-Tetzlaff, A., Waser, L. T., Haeni, M., & Meier, R. (2020). Increasing the broad-leaved tree fraction in European forests mitigates hot temperature extremes. *Scientific Reports*, 10(1), 1–9. <https://doi.org/10.1038/s41598-020-71055-1>
- Siriri, D., Wilson, J., Coe, R., Tenywa, M. M., Bekunda, M. A., Ong, C. K., & Black, C. R. (2013). Trees improve water storage and reduce soil evaporation in agroforestry systems on bench terraces in SW Uganda. *Agroforestry Systems*, 87(1), 45–58. <https://doi.org/10.1007/s10457-012-9520-x>
- Smith, A., Tetzlaff, D., Gelbrecht, J., Kleine, L., & Soulsby, C. (2020). Riparian wetland rehabilitation and beaver re-colonization impacts on hydrological processes and water quality in a lowland agricultural catchment. *Science of the Total Environment*, 699(September 2019), 134302. <https://doi.org/10.1016/j.scitotenv.2019.134302>
- Smith, A., Tetzlaff, D., Kleine, L., Maneta, M., & Soulsby, C. (2021). Quantifying the effects of land use and model scale on water partitioning and water ages using tracer-aided ecohydrological models [dataset]. *Hydrology and Earth System Sciences*, 25(6), 3635–3652. <https://doi.org/10.5194/hess-25-3635-2021>
- Smith, A., Tetzlaff, D., Landgraf, J., Dubbert, M., & Soulsby, C. (2022). Modelling temporal variability of in situ soil water and vegetation isotopes reveals ecohydrological couplings in a riparian willow plot. *Biogeosciences*, 19(9), 2465–2485. <https://doi.org/10.5194/bg-19-2465-2022>
- Smith, A., Tetzlaff, D., Laudon, H., Maneta, M., & Soulsby, C. (2019). Assessing the influence of soil freeze-thaw cycles on catchment water storage-flux-age interactions using a tracer-aided ecohydrological model. *Hydrology and Earth System Sciences*, 23(8), 3319–3334. <https://doi.org/10.5194/hess-23-3319-2019>
- Smith, A., Tetzlaff, D., Maneta, M., & Soulsby, C. (2022a). Critical zone response times and water age relationships under variable catchment wetness states: Insights using a tracer-aided ecohydrological model. *Water Resources Research*, 58, e2021WR030584. <https://doi.org/10.1029/2021wr030584>
- Smith, A., Tetzlaff, D., Maneta, M., & Soulsby, C. (2022b). Visualizing catchment-scale spatio-temporal dynamics of storage-flux-age interactions using a tracer-aided ecohydrological model. *Hydrological Processes*, 36(2), 8–10. <https://doi.org/10.1002/hyp.14460>
- Sohier, H., Farges, J.-L., & Piet-Lahanier, H. (2014). Improvement of the representativity of the morris method for air-launch-to-orbit separation. *IFAC Proceedings Volumes*, 47(3), 7954–7959.
- Soulsby, C., Birkel, C., Geris, J., Dick, J., Tunaley, C., & Tetzlaff, D. (2015). Stream water age distributions controlled by storage dynamics and nonlinear hydrologic connectivity: Modeling with high-resolution isotope data. *Water Resources Research*, 51(9), 7759–7776.
- Sprenger, M., Stumpp, C., Weiler, M., Aeschbach, W., Allen, S. T., Benettin, P., Dubbert, M., Hartmann, A., Hrachowitz, M., Kirchner, J. W., McDonnell, J. J., Orlowski, N., Penna, D., Pfahl, S., Rinderer, M., Rodriguez, N., Schmidt, M., & Werner, C. (2019). The demographics of water: A review of water ages in the critical zone. *Reviews of Geophysics*, 57(3), 800–834.
- Tague, C., & Frew, J. (2021). Visualization and ecohydrologic models: Opening the box. *Hydrological Processes*, 35(1), 1–13. <https://doi.org/10.1002/hyp.13991>
- Vose, J. M., Sun, G., Ford, C. R., Bredemeier, M., Otsuki, K., Wei, X., Zhang, Z., & Zhang, L. (2011). Forest ecohydrological research in the 21st century: What are the critical needs? *Ecohydrology*, 4(2), 146–158.
- Vrugt, J. A., Ter Braak, C. J. F., Gupta, H. V., & Robinson, B. A. (2009). Equifinality of formal (DREAM) and informal (GLUE) Bayesian approaches in hydrologic modeling? *Stochastic Environmental Research and Risk Assessment*, 23(7), 1011–1026. <https://doi.org/10.1007/s00477-008-0274-y>
- Wright, A. J., Mommer, L., Barry, K., & Van Ruijven, J. (2021). Stress gradients and biodiversity: Monoculture vulnerability drives stronger biodiversity effects during drought years. *Ecology*, 102(1), 1–10. <https://doi.org/10.1002/ecy.3193>
- Wu, S., Tetzlaff, D., Goldhammer, T., Freymueller, J., & Soulsby, C. (2022). Tracer-aided identification of hydrological and biogeochemical controls on in-stream water quality in a riparian wetland. *Water Research*, 222, 118860.
- Wu, S., Tetzlaff, D., Goldhammer, T., & Soulsby, C. (2021). Hydroclimatic variability and riparian wetland restoration control the hydrology and nutrient fluxes in a lowland agricultural catchment. *Journal of Hydrology*, 603, 126904.
- Wu, W., Kuang, L., Li, Y., He, L., Mou, Z., Wang, F., Zhang, J., Wang, J., Li, Z., Lambers, H., Sardans, J., Peñuelas, J., Geisen, S., & Liu, Z. (2021). Faster recovery of soil biodiversity in native species mixture than in eucalyptus monoculture after 60 years afforestation in tropical degraded coastal terraces. *Global Change Biology*, 27(20), 5329–5340. <https://doi.org/10.1111/gcb.15774>
- Xu, Z., Li, L., & Zhao, J. (2017). A distributed eco-hydrological model and its application. *Water Science and Engineering*, 10(4), 257–264. <https://doi.org/10.1016/j.wse.2017.12.007>
- Yang, X., Tetzlaff, D., Müller, C., Knöller, K., Borchardt, D., & Soulsby, C. (2023). Upscaling tracer-aided ecohydrological modeling to larger catchments: Implications for process representation and heterogeneity in landscape organization. *Water Resources Research*, 59(3), e2022WR033033.
- Yang, X., Tetzlaff, D., Soulsby, C., Smith, A., & Borchardt, D. (2021). Catchment functioning under prolonged drought stress: Tracer-aided ecohydrological modeling in an intensively managed agricultural catchment. *Water Resources Research*, 57(3), 1–23. <https://doi.org/10.1029/2020WR029094>
- Ying, Z., Tetzlaff, D., Freymueller, J., Comte, J. C., Goldhammer, T., Schmidt, A., & Soulsby, C. (2024). Developing a conceptual model of groundwater–Surface water interactions in a drought sensitive lowland catchment using multi-proxy data. *Journal of Hydrology*, 628, 130550.
- Zhou, X., Sheng, Z., Yang, Y., Han, S., Zhang, Q., Li, H., & Yang, Y. (2022). Catchment water storage dynamics and its role in modulating streamflow generation in spectral perspective: A case study in the headwater of Baiyang Lake, China. *Hydrology and Earth System Sciences Discussions*, 2022(2022):1–28.

## SUPPORTING INFORMATION

Additional supporting information can be found online in the Supporting Information section at the end of this article.

**How to cite this article:** Luo, S., Tetzlaff, D., Smith, A., & Soulsby, C. (2024). Assessing impacts of alternative land use strategies on water partitioning, storage and ages in drought-sensitive lowland catchments using tracer-aided ecohydrological modelling. *Hydrological Processes*, 38(4), e15126. <https://doi.org/10.1002/hyp.15126>